



Chinese Pharmaceutical Association  
Institute of Materia Medica, Chinese Academy of Medical Sciences

Acta Pharmaceutica Sinica B

[www.elsevier.com/locate/apsb](http://www.elsevier.com/locate/apsb)  
[www.sciencedirect.com](http://www.sciencedirect.com)



ORIGINAL ARTICLE

# Hyperglycemia activates FGFR1 *via* TLR4/c-Src pathway to induce inflammatory cardiomyopathy in diabetes



Xiong Chen<sup>a,b,c,†</sup>, Jinfu Qian<sup>d,†</sup>, Shiqi Liang<sup>b,d</sup>, Jianchang Qian<sup>b</sup>,  
Wu Luo<sup>b</sup>, Yujuan Shi<sup>a,b</sup>, Hong Zhu<sup>a</sup>, Xiang Hu<sup>a</sup>, Gaojun Wu<sup>d</sup>,  
Xiaokun Li<sup>b,c</sup>, Guang Liang<sup>a,b,e,\*</sup>

<sup>a</sup>Department of Endocrinology, the First Affiliated Hospital, Wenzhou Medical University, Wenzhou 325035, China

<sup>b</sup>Chemical Biology Research Center, School of Pharmaceutical Sciences, Wenzhou Medical University, Wenzhou 325035, China

<sup>c</sup>Department of Wound Repair, the First Affiliated Hospital, Wenzhou Medical University, Wenzhou 325035, China

<sup>d</sup>Department of Cardiology, the First Affiliated Hospital, Wenzhou Medical University, Wenzhou 325035, China

<sup>e</sup>School of Pharmaceutical Sciences, Hangzhou Medical College, Hangzhou 311399, China

Received 29 September 2023; received in revised form 11 December 2023; accepted 5 January 2024

## KEY WORDS

Diabetic cardiomyopathy;  
Protein tyrosine kinases;  
FGFR1;  
Cardiomyocytes;  
Inflammatory responses;  
Toll-like receptor 4;  
c-Src;  
NFκB

**Abstract** Protein tyrosine kinases (RTKs) modulate a wide range of pathophysiological events in several non-malignant disorders, including diabetic complications. To find new targets driving the development of diabetic cardiomyopathy (DCM), we profiled an RTKs phosphorylation array in diabetic mouse hearts and identified increased phosphorylated fibroblast growth factor receptor 1 (p-FGFR1) levels in cardiomyocytes, indicating that FGFR1 may contribute to the pathogenesis of DCM. Using primary cardiomyocytes and H9C2 cell lines, we discovered that high-concentration glucose (HG) transactivates FGFR1 kinase domain through toll-like receptor 4 (TLR4) and c-Src, independent of FGF ligands. Knocking down the levels of either TLR4 or c-Src prevents HG-activated FGFR1 in cardiomyocytes. RNA-sequencing analysis indicates that the elevated FGFR1 activity induces pro-inflammatory responses *via* MAPKs–NFκB signaling pathway in HG-challenged cardiomyocytes, which further results in fibrosis and hypertrophy. We then generated cardiomyocyte-specific FGFR1 knockout mice and showed that a lack of FGFR1 in cardiomyocytes prevents diabetes-induced cardiac inflammation and preserves cardiac function in mice. Pharmacological inhibition of FGFR1 by a selective inhibitor, AZD4547, also prevents cardiac inflammation, fibrosis, and dysfunction in both type 1 and type 2 diabetic mice. These studies

\*Corresponding author.

E-mail address: [wzmlianguang@163.com](mailto:wzmlianguang@163.com) (Guang Liang).

†These authors made equal contributions to this work.

Peer review under the responsibility of Chinese Pharmaceutical Association and Institute of Materia Medica, Chinese Academy of Medical Sciences.

<https://doi.org/10.1016/j.apsb.2024.01.013>

2211-3835 © 2024 The Authors. Published by Elsevier B.V. on behalf of Chinese Pharmaceutical Association and Institute of Materia Medica, Chinese Academy of Medical Sciences. This is an open access article under the CC BY-NC-ND license (<http://creativecommons.org/licenses/by-nc-nd/4.0/>).

have identified FGFR1 as a new player in driving DCM and support further testing of FGFR1 inhibitors for possible cardioprotective benefits.

© 2024 The Authors. Published by Elsevier B.V. on behalf of Chinese Pharmaceutical Association and Institute of Materia Medica, Chinese Academy of Medical Sciences. This is an open access article under the CC BY-NC-ND license (<http://creativecommons.org/licenses/by-nc-nd/4.0/>).

## 1. Introduction

Diabetic cardiomyopathy (DCM) is a diabetes-specific, distinct myocardial disease that entails ventricular dysfunction and leads to heart failure<sup>1,2</sup>. Soon after its discovery in 1972, hallmarks of silent diabetic cardiomyopathy (subclinical structural changes) emerged as diffuse myocardial fibrosis, cardiac hypertrophy, and microangiopathy. Clinical management of patients with DCM remains a challenge, and effective treatments are still lagging<sup>3</sup>. This is, in part, due to our incomplete understanding of the disease pathobiology. Metabolic derangements in diabetes affect most of the cells including cardiomyocytes and cardiac fibroblasts in the heart. Valuable insight into the mechanisms leading to structural and functional cardiac deficits has come from human studies and preclinical animal models of diabetes. For example, we now know that excessive reactive oxygen species, atypical activation of poly (ADP-ribose) polymerase and protein kinase C, accumulated advanced glycation end products, altered fatty acid metabolism, and unregulated renin-angiotensin system may, in part, play a role<sup>4</sup>. More recently, the innate immune system<sup>5</sup> and chronic inflammation<sup>6</sup> have emerged as critical to the development and progression of DCM. Despite these advances, we still need a greater understanding of the mechanisms and to identify suitable targets that can be modulated to affect disease trajectory.

Protein tyrosine kinases (PTKs) modulate a wide range of cellular events under normal cell conditions and in diseased states. PTKs are therefore important targets for basic research and drug development. Tyrosine kinase inhibitors (TKIs) have proven efficacy for the treatment of oncological disorders<sup>7</sup>. There is additional evidence that PTK signalling also has an important pathophysiological role in non-malignant diseases such as cardiac hypertrophy, pulmonary hypertension, lung fibrosis, rheumatoid disorders, atherosclerosis, and glomerulonephritis<sup>8</sup>. Several reports from clinical observations, animal models, and *in vitro* studies have documented the effect of TKIs in diabetes and its complications<sup>9,10</sup>. Tsatsoulis et al.<sup>11</sup> reviewed that targeting several PTKs may provide novel approaches for correcting the pathophysiologic disturbances of diabetes. Especially, recent studies in animal models of diabetes have shown an involvement of epidermal growth factor receptor, a receptor tyrosine kinase, in diabetic nephropathy<sup>12</sup> and cardiomyopathy<sup>13–15</sup>. The plethora of diabetes-induced biochemical changes in heart tissues prompts utilizing a slightly different approach to find key signaling proteins. One possible approach may be to screen for PTKs using a kinome profiling array, as PTKs play essential functions and may converge a range of signals in DCM.

In the present study, we profiled PTK phosphorylation in heart tissues of diabetic mice in an unbiased manner and identified increased phospho-fibroblast growth factor receptor 1 (p-FGFR1) levels in cardiomyocytes. FGFR1 is a receptor tyrosine kinase and has been well demonstrated as a therapeutic target for cancer

treatment<sup>16,17</sup>. Several small-molecule FGFR1 inhibitors have been successfully applied in clinical cancer therapy<sup>18,19</sup>. Although there is a plethora of information on the growth-promoting effects of FGFR1, limited studies have been performed on the role of FGFR1 in the development of non-malignant diseases<sup>20,21</sup>. For instance, reports indicate that the FGFR activation in macrophages may contribute significantly to atherosclerotic lesion growth<sup>22</sup>. However, the role of FGFR1 in the pathogenesis of DCM is unknown. Since at least 4 FGFR1 inhibitors have been used in clinical cancer therapy, the demonstration of the benefits of FGFR1 blockade in DCM may provide new references for their clinical applications.

Here, we show that high-concentration glucose (HG) induces activating FGFR1 phosphorylation through engaging toll-like receptor 4 (TLR4), part of the innate immune system, and c-Src in cardiomyocytes. HG-activated FGFR1 signaling led to the induction of inflammatory responses and excessive cardiomyocyte remodeling *via* the mitogen-activated protein kinase (MAPKs)/NF $\kappa$ B pathway. Importantly, either cardiomyocyte-specific FGFR1 knockout or pharmacological FGFR1 inhibition showed remarkable protection against diabetes-induced cardiac inflammation, structural alterations, and functional deficits in mice. These studies have identified a novel role and mechanism of FGFR1 in diabetic cardiomyopathy, and suggest that targeting FGFR1 may be able to combat cardiac dysfunction in diabetes.

## 2. Materials and methods

### 2.1. General reagents

D-(+)-Glucose (G8270), DAPI (D9542), 2-deoxy-D-glucose (2-DG, D6134), and streptozotocin (STZ, S0130) were purchased from Sigma–Aldrich (St. Louis, MO, USA). Mannitol (MNT, M119324) was purchased from Aladdin (Shanghai, China). Rhodamine phalloidin (ab176756) was purchased from Abcam (Cambridge, UK). Lipofectamine 3000 (L3000001) was purchased from Thermo Fisher (Waltham, MA, USA). Polyethyleneimine (PEI, 23966-1) was purchased from Polysciences (Warrington, PA, USA). Antibodies against GAPDH (sc-365062), phospho-c-Src (Tyr530/535, sc-166860), c-Src (sc-8056), TLR4 (sc-293072), glucose transporter-4 (GLUT4, sc-53566), atrial natriuretic peptide (ANP, sc-515701), skeletal and cardiac myosin heavy chain (MYH, sc-376157) and alpha-actinin ( $\alpha$ -actinin, sc-17829) were purchased from Santa Cruz Biotechnology (Dallas, TX, USA). Antibodies directed against phospho-FGF receptor 1 (Tyr766, 2544s), phospho-c-Jun (Ser73, 3270), phospho-NF- $\kappa$ B p65 (Ser536, 3033), NF- $\kappa$ B p65 (8242S), JNK1/2 (9252), phospho-JNK1/2 (Thr183/Tyr185, 9255), p38 MAPK (9212), phospho-p38 MAPK (Thr180/Tyr182, 9211S), p44/42 MAPK (ERK1/2, 4695), and phospho-p44/42 MAPK (Thr202/Tyr204,

4370) were obtained from Cell Signaling (Danvers, MA, USA). Antibodies against FGFR1 (ab76464), Vimentin (ab8978), RAGE (sc-ab3611), TGF- $\beta$ 1 (TGFB1, ab92486), collagen I (COL-1, ab34710), and c-Jun (ab32137) were purchased from Abcam. Antibodies against GLUT1 (21829-1-AP), His-tag (66005-1-Ig), and I $\kappa$ B alpha (I $\kappa$ B $\alpha$ , 10268-1-AP) was obtained from Proteintech (Rosemont, IL, USA). Anti-mouse IgG, HRP-linked (7076), and anti-rabbit IgG, HRP-linked (7074) were obtained from Cell Signaling. Goat anti-rabbit IgG H&L (TRITC, ab6718), and goat anti-mouse IgG H&L (Alexa Fluor 488, ab150117) were purchased from Abcam. Selective FGFR1 inhibitor AZD4547 (S2801), p38 inhibitor SB203580 (S1076), ERK inhibitor SCH772984 (S7101), and JNK inhibitor SP600125 (S1460) were purchased from Selleck Chemicals (Houston, TX, USA). These inhibitors were dissolved in dimethyl sulfoxide (DMSO) for *in vitro* studies.

## 2.2. Cell isolation and culture

Embryonic rat heart-derived H9C2 cells and human embryonic kidney 293 cells (HEK-293T) were obtained from the Shanghai Institute of Biochemistry and Cell Biology (Shanghai, China). Cells were cultured in Dulbecco's modified Eagle's medium (DMEM, Gibco/BRL Life Technologies, Eggenstein, Germany) containing 1 g/L glucose. Media was supplemented with 10% heat-inactivated fetal bovine serum (FBS, Thermo Fisher, Waltham, MA, USA), 100 U/mL penicillin, and 100 mg/mL streptomycin.

Isolation and culture of neonatal rat cardiomyocytes were performed as described previously<sup>23</sup>. The protocol used to isolate neonatal rat and mouse cardiomyocytes is nearly identical. Briefly, heart tissues from neonatal Sprague–Dawley rats were harvested and dissociated with trypsin. Cell suspension was plated for 1 h on tissue culture dishes in DMEM supplemented with 10% FBS. This pre-plating removes fibroblasts and endothelial cells. Non-adherent cells were then collected and plated on 6-well culture plates. Primary cardiomyocytes were cultured in the same growth medium as H9C2 cells.

Isolation and culture of adult mouse left ventricular cardiomyocytes and cardiac fibroblasts were performed as described previously<sup>24</sup>. In brief, mice were anesthetized, and the chest was opened to expose the heart. The descending aorta was cut, and the heart was immediately flushed with 7 mL Ethylene diamine tetraacetic acid (EDTA) buffer through the right ventricle. Heart tissues were then transferred to 60-mm dishes containing fresh EDTA buffer. Digestion was achieved by sequential injection of 10 mL EDTA buffer, 3 mL perfusion buffer (EDTA-free), and 50 mL collagenase buffer (0.5 mg/mL collagenase 2, 0.5 mg/mL collagenase 4, 0.05 mg/mL protease XIV) into the left ventricle using a peristaltic pump. Tissues were pulled apart into 1-mm pieces. Cellular dissociation was completed by gentle trituration, and enzyme activity was inhibited by the addition of a 5 mL stop buffer. Cardiac myocytes underwent 4 sequential rounds of gravity settling, using 3 intermediate calcium reintroduction buffers to gradually restore calcium concentration to physiological levels. Fibroblasts were isolated from the supernatant remaining after the initial 10 min settling phase of cardiac myocytes. Cells were centrifuged at 250 $\times$ g for 5 min. Cell pellets were resuspended in DMEM 1 g/L glucose +10% FBS and then placed directly into 6-well plates. After 6 h, non-adherent cells (cardiac myocytes) were washed with PBS 3 times, adherent cells (fibroblasts) were cultured, and the media was changed every 48 h.

In cellular experiments, cultured cells were challenged with HG at 33 mmol/L for the indicated time. This concentration of glucose is selected according to our previous studies<sup>25</sup> and a lot of studies conducted by other groups<sup>26,27</sup>.

## 2.3. Kinase and phospho-kinase arrays

Kinase Antibody Array Kit (AVK276, including 276 kinase antibodies) and Tyrosine Phosphorylation ProArray (PST228, including 228 site-specific tyrosine phosphorylation antibodies) were obtained from Full Moon Biosystems (Sunnyvale, CA USA)<sup>28</sup>. Protein microarray analysis was carried out by Wayen Biotechnologies (Shanghai, China). Briefly, proteins from the heart tissues of control or type 1 diabetic mice were extracted and labeled with Biotin. The samples were diluted 1:20 in coupling solution before being applied to the array for conjugation. Arrays were washed three times, and Cy3-Streptavidin was used for detection. Slides were scanned using the GenePix 4000B Array Scanner (Axon Instruments, Foster City, CA, USA). The analyzed results were expressed by the ratio of phosphorylated/total protein.

## 2.4. Animal experiments

All animal care and experimental procedures were approved by the Wenzhou Medical University Animal Policy and Welfare Committee (Approval Document No. wydw2018-0224). All animals received humane care according to the National Institutes of Health (USA) guidelines. Six-week-old male C57BL/6 mice were obtained from the Animal Center of Wenzhou Medical University. The *Fgfr1*<sup>fl $ox$</sup>  mice on C57BL/6 background were kindly provided by Professor Lin Chen at the Third Military Medical University (Chongqing, China).  $\alpha$ MHC-MerCreMer mice, which have cardiac-specific alpha-MHC (Myh6) directing the expression of a tamoxifen-inducible Cre recombinase (MerCreMer), were obtained by Jackson Laboratory (Stock# 005650; Bar Harbor, ME, USA). Adult male leptin receptor-deficient (*db/db*) mice and their non-diabetic littermates (*db/m*) mice were purchased from Beijing Vital River Laboratory Animal Technology Co., Ltd. (Beijing, China). Mice were housed at a constant room temperature with a 12:12 h light–dark cycle and fed with a standard rodent diet in the Animal Centre of Wenzhou Medical University. The animals were acclimatized to the laboratory for at least 2 weeks before initiating the studies. All animal experiments were performed and analyzed by blinded experimenters. Randomization was used when dividing the groups.

- (1) Treatment with FGFR1 inhibitor in STZ-induced type 1 diabetic mice. Type 1 diabetes was induced by intraperitoneal injection of 50 mg/kg/day STZ (dissolved in citrate buffer, pH 4.5) for five days consecutive in 8-week-old male mice. The control group received the same volume of citrate buffer. Control mice (Ctrl,  $n = 7$ ) received citrate buffer alone. Two weeks after STZ injection, mice with a fasting blood glucose concentration greater than 12 mmol/L were considered diabetic and used in the study. Diabetic mice were randomly divided into two groups: untreated diabetic mice (STZ,  $n = 7$ ), and diabetic mice treated with 5 mg/kg AZD4547 (STZ + AZD,  $n = 7$ ). AZD4547 was administered every other day by oral gavage for 20 weeks. Mice in Ctrl and STZ groups received 1% CMC-Na solution in the same schedule. Blood glucose levels and body weights were recorded regularly.

- (2) Treatment with FGFR1 inhibitor in *db/db* type 2 diabetic mice. Eight-week-old *db/db* male mice were randomly divided into two groups: untreated diabetic mice (*db/db*,  $n = 6$ ), and diabetic mice treated with 5 mg/kg AZD4547 (*db/db* + AZD,  $n = 6$ ). *db/m* mice were used as non-diabetic control mice (*db/m*,  $n = 6$ ). AZD4547 was administered every other day by oral gavage for 8 weeks. Mice in *db/m* and *db/db* groups received 1% CMC-Na solution in the same schedule. Blood glucose levels and body weights were recorded regularly.
- (3) Cardiomyocyte-specific FGFR1 knockout mice. To generate tamoxifen-inducible cardiomyocyte-specific FGFR1 knockout mice (*Fgfr1<sup>ΔCM</sup>* mice), we crossed *Fgfr1<sup>fllox</sup>* mice with MHC-MerCreMer mice using the Cre-loxP method. Cre was activated by intraperitoneal injection of tamoxifen (75 mg/kg, 5 consecutive days) in 6-week-old *Fgfr1<sup>ΔCM</sup>* mice. Mice were allowed to recover for 9 days before administering STZ. Type 1 diabetes in 8-week-old *Fgfr1<sup>fllox</sup>* and *Fgfr1<sup>ΔCM</sup>* mice was induced by intraperitoneal injection of 50 mg/kg/day STZ for five consecutive days. Two weeks after STZ injection, mice with a fasting blood glucose concentration greater than 12 mmol/L were considered diabetic and used in the study (*Fgfr1<sup>fllox</sup>* + STZ group,  $n = 7$ ; *Fgfr1<sup>ΔCM</sup>* + STZ group,  $n = 7$ ). Mice were maintained at diabetic status for 28 weeks to induce diabetic cardiomyopathy. *Fgfr1<sup>fllox</sup>* mice ( $n = 6$ ) were injected with citrate buffer. Blood glucose levels and body weights were recorded regularly.

Before sacrificing mice, heart function was assessed by Doppler ultrasound. Mice were anesthetized with isoflurane and echocardiography was performed by SONOS 5500 ultrasound (Philips Electronics, Amsterdam, Netherlands) with a 15-MHz linear array ultrasound transducer. At the end of treatment, mice were sacrificed under sodium pentobarbital (i.p. injection of pentobarbital at 50 mg/kg) for anesthesia and pain medication. The blood and hearts were collected for subsequent analyses.

### 2.5. Heart tissue histology and immunostaining

Heart tissues were fixed in 4% paraformaldehyde, embedded in paraffin, and sectioned at 5- $\mu$ m thickness. Sections were stained with hematoxylin and eosin (H&E) for histopathological assessment. Cardiomyocyte size was evaluated in cross-sections of heart tissues. Sections were also stained with Masson's Trichrome (Beyotime Biotech, Nantong, China) and Picro Sirius Red (Beyotime Biotech, Nantong, China) to assess cardiac fibrosis.

For immunofluorescence staining, 5- $\mu$ m tissue sections were permeabilized with 0.25% Triton X-100 for 10 min and blocked with 5% bovine serum albumin for 30 min at 37 °C. Samples were then incubated with primary antibodies at 4 °C overnight. Antibodies included p-FGFR1 (1:200), FGFR1 (1:200),  $\alpha$ -Actinin (1:100), and Vimentin (1:200). Fluorophore-conjugated secondary antibodies were used for detection. Slides were counterstained with DAPI for 5 min. Images were taken using the Nikon A1 laser confocal microscope (Nikon, Japan).

For immunohistochemical staining, 5- $\mu$ m tissue sections were deparaffinized, rehydrated, treated with 3% H<sub>2</sub>O<sub>2</sub> for 30 min to block endogenous peroxidase activity, and blocked with 5% bovine serum albumin for 30 min. Slides were incubated with

primary antibodies (CD68, 1:200) at 4 °C overnight. Peroxidase-conjugated secondary antibodies were used for detection (1:200 dilution, 1 h incubation). Slides were counterstained with hematoxylin for 5 min, dehydrated, and mounted for viewing by brightfield microscopy (Nikon, Japan).

### 2.6. Cell transfections for gene knockdown, mutagenesis, or over-expression

*Fgfr1*, *C-src*, *Tlr4*, *Glut4*, *Glut1* and *Rage* were silenced in H9C2 cells by siRNA transfections. The siRNA sequences were purchased from Gene Pharma Co., Ltd. (Shanghai, China) and shown in [Supporting Information Table S1](#). Negative control transfections included scrambled siRNA sequences. All transfections were carried out using Lipofectamine 3000 (Thermo Fisher, Shanghai, China). Knockdown of genes in the transfected cells was confirmed by Western blot analysis.

For some experiments, His-tagged human FGFR1 and mutant FGFR1 were transfected in cells. For this, pCMV-SPORT6-human FGFR1 plasmid (NM\_001174063.1, P4917) was purchased from the MiaoLing Plasmid Sharing Platform (MLPSP, Wuhan, China). pcDNA 3.1 expression vectors encoding full-length His-tagged human FGFR1(1–822) and a truncated mutant ( $\Delta$ 22–376) were constructed using ClonExpress Ultra One Step Cloning Kit (C115-01, Vazyme Biotechnology, Nanjing, China). Primers for truncated mutagenesis are listed in [Supporting Information Table S2](#). All DNA constructs used were verified by DNA sequencing at Sangon Biotech (Shanghai, China). HEK-293T cells were transfected with plasmids using PEI (23966-1, Polysciences, PA, USA). A transfection complex was produced with PEI ( $\mu$ g) and plasmid ( $\mu$ g) at a 3:1 ratio in Opti MEM medium (31985062, Thermo Fisher). Cells were incubated with the transfection complex for 6 h. Media was replaced with a fresh growth medium.

To construct Y766A mutant FGFR1, PCR cloning was used to amplify Flag-*Fgfr1* and 5' (KpnI) and 3' (AgeI) were added. Y766A mutant *Fgfr1* was cloned into vector Flag-*Fgfr1* by the enzyme site 5' (KpnI) and 3' (AgeI) and then constructed into a mutated plasmid (*Fgfr1* Y766A). The plasmid was transfected into cells *via* Lipofectamine 3000.

The pReceiver-Lv121 vector was used to express the wide-type full-length *Fgfr1*. FGFR1 expression construct was generated by subcloning PCR-amplified full-length *Fgfr1* cDNA into the pReceiver-Lv121 plasmid (EX-Rn10315-Lv121, Biosea Biotechnology, Hangzhou, China). The length of the *Fgfr1* open reading frame (ORF) was 2469 bp. A plasmid carrying a non-targeting sequence was used as a negative control. For lentiviral production, the lentiviral expression vector was co-transfected with lentivirus packing vectors into HEK-293T cells using Lipofectamine 3000. Target cells were transduced and stable lines expressing FGFR1 were selected following puromycin culture for 72 h. The medium was removed after 48 h and replaced with a complete culture medium.

### 2.7. Rhodamine phalloidin staining of cultured cells

To assess cardiomyocyte hypertrophy, cells in culture were fixed with 4% paraformaldehyde, permeabilized with 0.1% Triton X-100, and stained with rhodamine phalloidin at 50  $\mu$ g/mL for 30 min. Nuclei were stained with the DAPI at room temperature.

Immunofluorescence staining was viewed and captured using a Nikon epifluorescence microscope (Nikon, Japan).

## 2.8. Surface plasmon resonance (SPR) analysis

The potential binding of glucose and recombinant FGF2 to FGFR1 was determined using the Biacore T200 Protein Interaction Assay system (GE Healthcare, MA, USA) with a CM7 sensor chip (29-1470-20). Recombinant human FGFR1 protein (rhFGFR1) was dissolved in 10 mmol/L acetate acid buffer (pH 5.0). An amine coupling kit (GE BR-1000-50) was used to immobilize rhFGFR1 on the chip. Different concentrations of glucose, including 2000, 1000, 500, 250, 125, 62.5, 31.25, 15.6, and 7.8  $\mu\text{mol/L}$ , were prepared with running buffer (PBS containing 5% DMSO). Similarly, different concentrations of bFGF (CTP0263, Thermo Fisher) were prepared and included 100, 50, 25, 12.5, 6.25, 3.13, 1.56, 0.78 and 0.39  $\mu\text{mol/L}$ . Sensor and sample plates were placed in the instrument. The interactions were determined at a flow rate of 30  $\mu\text{L/min}$  for 180 s during the association phase, followed by 250 s for the dissociation phase at 25 °C. The data were analyzed with Biacore T200 manager software. Binding kinetic parameters were calculated by global fitting of the kinetic data from various concentrations of glucose and bFGF using a 1:1 Langmuir binding model.

## 2.9. RNA sequencing (RNA-seq) and data analysis

Total RNA from H9C2 cells in four treated groups was prepared with Trizol (Thermo Fisher). RNA sequencing was performed by LC-Bio Inc., Hangzhou, China. For data analysis, differentially expressed genes were identified by using a *P*-adjust of 0.05 as a cutoff. Heat map analysis was performed with OmicStudio tools (<https://www.omicstudio.cn/>). Gene Ontology (GO) enrichment analysis was performed with R software (Version 3.5.3). TRRUST Transcription Factors analysis was performed with modEnrichr (<https://amp.pharm.mssm.edu/modEnrichr/>).

## 2.10. Western blot and immunoprecipitation

Lysates from cultured cells and mouse heart tissues were prepared and protein concentrations were determined by the Bradford assay (Bio-Rad Laboratories, Hercules, CA, USA). Samples were separated using sodium dodecyl sulfate-polyacrylamide gel electrophoresis, and electro-transferred to nitrocellulose membranes. Membranes were then blocked for 1.5 h at room temperature in Tris-buffered saline (pH 7.6) containing 0.05% Tween 20 and 5% non-fat dry milk. Primary antibody incubations were carried out at 4 °C overnight. Secondary antibodies were applied for 1 h at room temperature. Immunoreactivity was visualized using enhanced chemiluminescence reagents (Bio-Rad Laboratories).

Protein complexes were evaluated by co-immunoprecipitation, coupled with immunoblotting. Cell lysates were incubated with precipitating antibody at 4 °C overnight. Samples were immunoprecipitated with protein A + G-Sepharose beads with shaking at room temperature for 2 h. Protein-bead complexes were washed five times with PBS, electrophoresed, transferred to PVDF membranes, and detected with immunoblotting antibody. Densitometric measurements were made using Image J version 1.38e (NIH, Bethesda, MD, USA).

## 2.11. Real-time quantitative PCR

Cells and heart tissues were homogenized in TRIZOL (Invitrogen, Shanghai, China). Both reverse transcription and quantitative PCR (qPCR) were carried out using a two-step M-MLV Platinum SYBR Green qPCR SuperMix-UDG kit (Invitrogen, Shanghai, China). Eppendorf Mastercycler<sup>®</sup> Ep Realplex detection system (Eppendorf, Hamburg, Germany) was used for qPCR analysis. The primers of target genes are listed in Supporting Information Tables S3 and S4 and were obtained from Invitrogen (Shanghai, China). The amount of each gene was determined and normalized to the amount of  $\beta$ -actin.

## 2.12. Chromatin immunoprecipitation (ChIP)-quantitative PCR

ChIP assay for NF $\kappa$ B transcriptional activity was performed using SimpleChIP enzymatic chromatin IP kit with magnetic beads (9003, Cell Signaling Technology). Quantitative PCR was performed with SYBR Green in the QuantStudio Real-Time PCR system (Thermo Fisher). Primers for NF $\kappa$ B promoter-binding sites were designed using Oligo 7 ([oligo.net](http://oligo.net)). Sequences are presented in Supporting Information Table S5.

## 2.13. Statistical analysis

Data presented in this study is representative of at least 3 independent experiments and is expressed as mean  $\pm$  SEM. The exact group size (*n*) for each experiment is provided and '*n*' refers to independent values, not technical replicates. Statistical analysis was performed with GraphPad Prism 8.0 software (San Diego, CA, USA). Comparisons between the two groups were analyzed by 2-tailed Student's *t*-test. We used one-way ANOVA followed by Tukey *post hoc* test when comparing more than two groups. *P* < 0.05 was considered statistically significant. Post-tests were run only if *F* achieved *P* < 0.05 and there was no significant variance inhomogeneity.

## 3. Results

### 3.1. Diabetes activates FGFR1 in cardiomyocytes

To further understand the pathobiology of diabetic cardiomyopathy and to identify potential therapeutic targets, we used a PST228 array featuring 228 site-specific phospho-tyrosine antibodies to probe the protein tyrosine phosphorylation in heart tissue lysates from non-diabetic control mice and STZ-induced diabetic mice. Analysis of the array studies showed a significantly increased level of phosphorylated p-FGFR1 (at Tyr-766) in diabetic heart samples (Fig. 1A and B). Tyr-766 is located in the C-terminal tail kinase domain of FGFR1 and is one of the important phosphorylation sites required for receptor function<sup>29</sup>. Using a similar AVK276 array approach, interestingly, we examined the levels of total FGFR1 and observed no significant difference between control and diabetic hearts (Fig. 1C). These studies indicate that, although the protein levels of FGFR1 may not change, there may be increased FGFR1 activity in the heart tissues of diabetic mice. We then confirmed increased p-FGFR1 in heart tissue lysates of diabetic mice using immunoblotting (Fig. 1D, Supporting Information Fig. S1A). To investigate the source of increased p-FGFR in diabetes, we stained the heart tissues and isolated cardiac fibroblasts and cardiomyocytes from the mouse tissues.

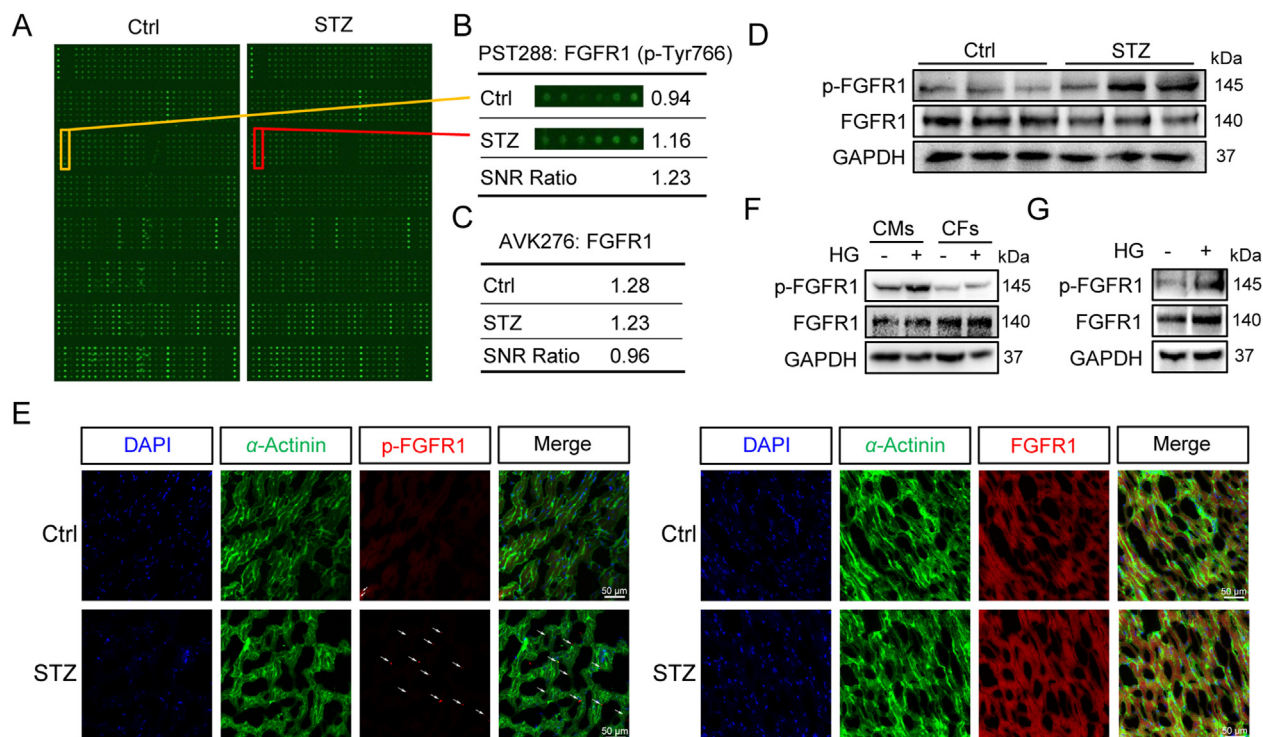


**Figure 1** Increased levels of phospho-FGFR1 in cardiomyocytes of diabetic mice. C57BL/6 mice were made diabetic by STZ. Heart tissues were harvested after 20 weeks of disease duration from diabetic (STZ) and non-diabetic control (Ctrl) mice. (A, B) Representative site-specific tyrosine kinase phosphorylation PST228 ProArray showing phosphorylated proteins (A). Magnified images and signal-to-noise ratio (SNR) of FGFR1 (Tyr766) in STZ (red box) and Ctrl (yellow box) are shown in panel (B). (C) Relative abundance of FGFR1 protein in STZ and Ctrl heart tissues from AVK276 Kinase Array were shown. (D) Representative blots showing the levels of p-FGFR1 (Tyr-766) and FGFR1 in heart tissue. GAPDH was used as a loading control. (E) Immunofluorescence staining of mouse heart tissues for p-FGFR1 (red), FGFR1 (red), and  $\alpha$ -actinin (green). Sections were counterstained with DAPI (blue). Arrows showing p-FGFR1-positive cells (Scale bar = 50  $\mu$ m). (F) Levels of p-FGFR1 (Tyr-766) and FGFR1 in primary adult mouse cardiomyocytes and cardiac fibroblasts. Cells were exposed to 33 mmol/L glucose (HG) for 15 min. GAPDH was used as loading control. (G) Levels of p-FGFR1 (Tyr-766) and FGFR1 in rat primary cardiomyocytes. Isolated cells were exposed to 33 mmol/L glucose (HG) for 15 min. GAPDH was used as loading control.

Double staining of mouse heart tissues for p-FGFR1 and  $\alpha$ -Actinin (a marker of cardiomyocytes) highlighted cardiomyocytes as the likely source of increased p-FGFR1 in diabetes (Fig. 1E, Fig. S1B). To confirm these findings, we also double-labeled heart tissues for p-FGFR1 and fibroblast marker vimentin. We found that p-FGFR1 primarily localizes to vimentin-negative cells in the heart tissues (Fig. S1C–S1E). Analysis of isolated adult mouse cardiac fibroblasts showed no significant increase in p-FGFR1 level when exposed to HG at 33 mmol/L in culture, but the p-FGFR1 level in HG-challenged mouse primary cardiomyocytes was found to be pronounced (Fig. 1F, Fig. S1F). As expected, FGFR1 phosphorylation was induced by HG in neonatal rat primary cardiomyocytes (Fig. 1G, Fig. S1G). These data indicate that cardiomyocytes may be the primary contributor to increased p-FGFR1 under the condition of HG/diabetes.

### 3.2. Cardiomyocyte FGFR1 activation by HG is mediated through TLR4 and c-Src

We first validated HG-activated FGFR1 in H9C2 cells. Immunoblotting showed increased p-FGFR1 in cells, in as early as 1–2 min of HG exposure (Fig. 2A, Supporting Information Fig. S2A). Mannitol at 33 mmol/L failed to activate FGFR1, excluding the effect of osmotic stress (Fig. S2B). This short

exposure was not associated with increased expression of FGF family ligands (Fig. S2C). Similarly, we did not observe altered expression of FGF ligands in diabetic mouse hearts compared to non-diabetic controls (Fig. S2D). Based on these results, we reasoned that HG may activate FGFR1 independent of FGF ligands following uptake into the cells (Fig. 2B). However, knocking down the expression of glucose transporter GLUT4 (Fig. 2C, Supporting Information Fig. S3A) did not prevent HG-induced FGFR1 phosphorylation (Fig. 2D, Fig. S3B), suggesting that extracellular glucose induces FGFR1 phosphorylation. In addition, silencing GLUT1 and receptor for advanced glycation end products (RAGE) in cardiomyocytes showed that HG-induced FGFR1 activation is also independent of GLUT1 and RAGE (Fig. S3C–S3F). These data indicate that HG-induced FGFR1 activation is independent of glucose uptake. Then, we examined if HG activates FGFR1 *via* binding to the extracellular domain of FGFR1. However, Surface Plasmon Resonance (SPR) analysis did not show any direct interaction between glucose and FGFR1 protein (Fig. 2E). For this assay, we used recombinant FGF2 as a positive comparison, and it showed direct interaction with FGFR1 (Fig. S3G). Furthermore, cells expressing either full-length FGFR1 or FGFR1 intracellular segments that lack extracellular portion ( $\Delta$ 22–376) showed HG-induced FGFR1 phosphorylation (Fig. 2F, Fig. S3H). These results indicate that 1)

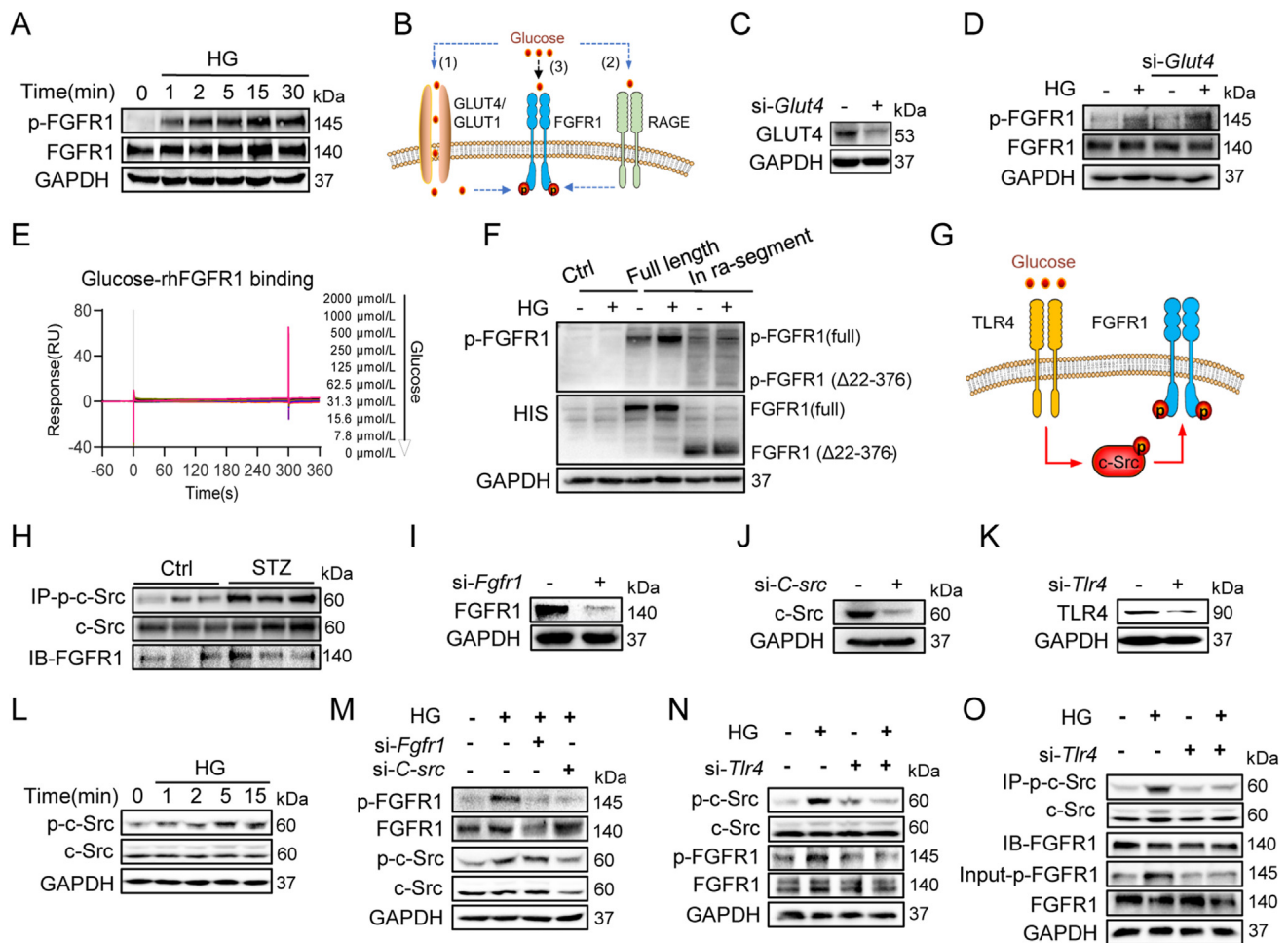


**Figure 2** Extracellular HG activates FGFR1 in cardiomyocytes by engaging TLR4. (A) H9C2 cells were exposed to 33 mmol/L glucose (HG). Levels of p-FGFR1 at Tyr-766 and total FGFR1 were determined at the indicated time points. GAPDH was used as a loading control. (B) Schematic illustrating the potential modes by which HG may activate FGFR1, including intracellular activation following uptake of glucose through GLUT4/GLUT1 (1) and RAGE (2) or extracellular activation (3). (C) Representative immunoblots showing levels of GLUT4 in H9C2 cells transfected with GLUT4 siRNA. GAPDH was used as a loading control. (D) Levels of p-FGFR1 induced by a 15-min HG exposure of H9C2 cells with or without GLUT4 siRNA. GAPDH was used as a loading control. (E) SPR analysis showing no direct interaction between rhFGFR1 and glucose. (F) HEK-293T cells were transfected with full-length FGFR1 (His-tagged) or truncated FGFR1 ( $\Delta 22-376$ ). Cells were exposed to HG for 15 min. Levels of p-FGFR1 and His-tag were measured by immunoblotting. (G) Schematic illustrating the possible involvement of TLR4 in FGFR1 activation by HG. (H) Heart tissue lysates from diabetic (STZ) and non-diabetic (Ctrl) were used to immunoprecipitate c-Src (IP). Immunoblotting (IB) for FGFR1 was then performed. (I) H9C2 cells were exposed to HG for up to 15 min. Protein levels of p-c-Src/c-Src were determined. GAPDH was used as a loading control. (J–L) Levels of FGFR1 (J), c-Src (K), and TLR4 (L) in H9C2 cells transfected with targeting siRNA. (M) H9C2 cells transfected with FGFR1 or c-Src siRNA were exposed to HG for 15 min. Levels of p-FGFR1 (Tyr-766) and p-c-Src were measured. (N) H9C2 transfected with TLR4 siRNA were exposed to HG for 15 min. Lysates were probed for p-FGFR1 and p-c-Src. (O) H9C2 cells were transfected with TLR4 siRNA and exposed to HG for 15 min. Lysates from cells were immunoprecipitated with p-c-Src antibody and probed for p-FGFR1.

extracellular HG indirectly activates FGFR1, and 2) HG induces intracellular FGFR1 kinase phosphorylation independent of FGFR1 extracellular domain.

Recent studies reported that lipopolysaccharide (LPS)-induced epidermal growth factor receptor transactivation occurs through TLR4 and c-Src<sup>30,31</sup>. We have also recently shown that HG directly activates TLR4 in the cell membrane of cardiomyocytes<sup>25</sup>. Thus, we hypothesize that FGFR1, possibly like EGFR, is transactivated by HG through TLR4/c-Src in cardiomyocytes (Fig. 2G). Indeed, lysates from heart tissues of diabetic mice showed increased interaction between p-c-Src and

FGFR1 (Fig. 2H, Supporting Information Fig. S4A), while no interaction between TLR4 and FGFR1 was detected (Fig. S4B). Exposure of cultured H9C2 cells to HG also induced p-c-Src rapidly (Fig. 2I, Fig. S4C), while 33 mmol/L mannitol could not activate c-Src phosphorylation (Fig. S4D). Knocking down the expression of GLUT4, GLUT1, or RAGE, respectively, did not affect HG-induced c-Src phosphorylation (Fig. S4E–S4G). We knocked down the expression of FGFR1, c-Src, and TLR-4 in H9C2 cells, respectively (Fig. 2J–L, Fig. S4H–S4J), and then exposed the cells to HG. We found that knocking down FGFR1 did not reduce HG-induced p-c-Src while silencing c-Src

blocked HG-induced FGFR1 phosphorylation (Fig. 2M, Fig. S4K). As expected, reduced expression of TLR4 was associated with reduced p-c-Src and p-FGFR1 levels (Fig. 2N, Fig. S4L). Furthermore, TLR4 knockdown reduced the interaction between c-Src and FGFR1 (Fig. 2O, Fig. S4M). Consistently, FGFR1 did not interact with TLR4 in H9c2 cells with or without HG stimulation (Fig. S4N). These data confirm that HG transactivates FGFR1 through TLR4 and c-Src in cardiomyocytes.

### 3.3. HG-induced FGFR1 mediates inflammatory injuries in cardiomyocytes

We proceeded to investigate the downstream consequences of FGFR1 activation by performing RNA-Seq in HG-challenged cardiomyocytes with or without FGFR1 knockdown. Seventy-seven genes appeared to be regulated by FGFR1 in the HG context through these comparisons (Fig. 3A, Supporting Information Fig. S5). GO analysis of these 77 genes showed that inflammatory pathways are mainly involved (Fig. 3B). qPCR assay validated these results by examining representative pro-inflammatory cytokine genes *Tnfa*, *Il6*, *Il1b*, *Il18*, *Icam1*, *Vcam1*, and *Ccl2*, which are involved in DCM<sup>32,33</sup>. We firstly validated the pro-inflammatory action of HG through qPCR assay of *Tnfa* and *Il6* and excluded the effect of osmotic stress using mannitol at the same concentration (Supporting Information Fig. S6A). Fig. 3C and Fig. S6B show a lack of *Tnfa*, *Il6*, *Il1b*, *Il18*, *Icam1*, *Vcam1*, and *Ccl2* induction by HG in H9C2 cells following FGFR1 knockdown. Since DCM manifests as augmented inflammatory responses in cardiomyocytes leading to hypertrophy and tissue fibrosis<sup>33</sup>, we probed for markers of these injuries in H9C2 cells exposed to HG. Firstly, we observed that HG induced the expression of fibrotic and hypertrophic proteins, while mannitol at 33 mmol/L failed (Fig. S6C). Then, we found that FGFR1 knockdown prevented HG-induced fibrosis-related proteins, collagen-1 (COL-1), and transforming growth factor-beta1 (TGF- $\beta$ 1) (Fig. 3D, Fig. S6D). Similarly, levels of cardiomyocyte hypertrophy markers, myosin heavy chain-beta ( $\beta$ -MyHC), and atrial natriuretic peptide (ANP) were suppressed in FGFR1 knockdown cells upon HG exposure (Fig. 3E, Fig. S6E). Furthermore, rhodamine staining of cells showed increased cell size upon HG exposure, while this increase was not seen when cells transfected with FGFR1 siRNA were exposed to HG (Fig. 3F, Fig. S6F). As described in Methods, we generated tamoxifen-inducible cardiomyocyte-specific FGFR1 knockout mice (Supporting Information Fig. S7A). We isolated the primary cardiomyocytes and cardiac fibroblasts from these adult mice. Fig. S7B shows that the conditional knockout mice (*Fgfr1*<sup>ΔCM</sup>) lack FGFR1 in cardiomyocytes, but not fibroblasts. Using the isolated cardiomyocytes from adult *Fgfr1*<sup>ΔCM</sup> or *Fgfr1*<sup>fllox</sup> mice, we validated that FGFR1 deficiency significantly prevented HG-induced over-expression of fibrotic and hypertrophic proteins in cardiomyocytes (Fig. S7C and S7D).

Although FGFR1 deletion unavoidably decreases the level of phosphorylated FGFR1, we further constructed plasmids encoding wide-type FGFR1 (*Fgfr1*<sup>WT</sup>) and Y766A mutant FGFR1 (*Fgfr1*<sup>Y766A</sup>), respectively, to better examine the role of FGFR1 phosphorylation in HG's actions. Plasmids encoding *Fgfr1*<sup>WT</sup> and *Fgfr1*<sup>Y766A</sup> proteins were transfected into FGFR1-deleted (*Fgfr1*-KO) H9c2 cells. Mutation of FGFR1 phosphorylating site (Y766A) abrogated HG-induced phosphorylation of FGFR1 in H9c2 cells (Fig. 3G, Supporting Information Fig. S8A). As shown

in Fig. 3H, I and Fig. S8B, the inactivation of FGFR1 by Y766A also suppressed HG-induced expression of COL-1, TGF- $\beta$ 1,  $\beta$ -MyHC, and ANP. Rhodamine staining of Ang II-challenged H9c2 cells with *Fgfr1*<sup>Y766A</sup> showed decreased hypertrophy compared to cells with *Fgfr1*<sup>WT</sup> (Fig. 3J, Fig. S8C). We also examined the effects of FGFR1 overexpression. Overexpression of FGFR1 using lenti-*Fgfr1* plasmid in H9C2 cells increased the level of FGFR1 phosphorylation (Fig. 3K, Supporting Information Fig. S9A), and then exaggerated the effects of HG and showed augmented inflammatory gene induction (Fig. 3L), fibrosis-associated proteins (Fig. 3M, Fig. S9B), and hypertrophic changes (Fig. 3N and O, Fig. S9C and S9D).

To confirm our findings, we performed similar studies upon pretreatment of H9C2 cells with a pharmacological inhibitor of FGFR1, AZD4547<sup>34</sup> (AZD; Supporting Information Fig. S10A). Our results show that AZD pretreatment mimics FGFR1 knockdown in preventing HG-induced inflammatory responses, fibrotic protein induction, and cellular hypertrophy in H9C2 cells (Fig. S10B–S10F). We further confirmed these findings in isolated adult mouse primary cardiomyocytes and neonatal rat primary cardiomyocytes, which are widely used in cardiac basic research<sup>26,35</sup>. Similar results were obtained when rat primary cardiomyocytes (Fig. S10G–S10K) or adult mouse primary cardiomyocytes (Fig. S10L and S10M) were pretreated with AZD and exposed to HG. Together, these data indicate that HG-induced FGFR1 activation mediates inflammatory responses and subsequent injuries in cardiomyocytes.

### 3.4. FGFR1 links HG to NF $\kappa$ B-mediated inflammatory responses

TRRUST Transcription Factors analysis of the RNA-seq data showed the potential involvement of NF $\kappa$ B, which ranked top 1 and 2 in the predicted transcription factor list (Fig. 4A). To determine whether FGFR1 is involved in HG-induced NF $\kappa$ B activation, we performed immunoblotting. Firstly, we observed that 33 mmol/L HG, but not mannitol, significantly induced the NF $\kappa$ B activation in H9c2 cells, measured through levels of p-p65 subunit and inhibitor of  $\kappa$ B $\alpha$  (I $\kappa$ B $\alpha$ ) (Supporting Information Fig. S11A). As anticipated, FGFR1 knockdown in HG-challenged H9C2 cells prevented p65 phosphorylation and I $\kappa$ B $\alpha$  degradation (Fig. 4B, Fig. S11B). Similar results were observed in H9C2 cells and rat primary cardiomyocytes treated with AZD4547 (Fig. 4C, Fig. S11C and S11D). Based on these results, we examined whether NF $\kappa$ B directly binds to the promoter regions of representative inflammatory genes *Tnfa* and *Il6*. Chromatin immunoprecipitation-qPCR assay showed HG-increased binding of NF $\kappa$ B to *Tnfa* and *Il6* promoters, while this binding was suppressed in H9C2 cells transfected with FGFR1 siRNA (Fig. 4D). In addition, inactive *Fgfr1*<sup>Y766A</sup> mutation also abrogated HG-induced p65 phosphorylation and I $\kappa$ B $\alpha$  degradation in H9c2 cells (Fig. 4E, Fig. S11E).

We then probed for the MAPKs pathway, since MAPKs have been reported to be downstream of FGFR1<sup>36,37</sup>, and meantime, to be an upstream regulator of NF $\kappa$ B. There is a close interaction between NF $\kappa$ B and MAPKs in cardiac injuries<sup>38</sup>. Then, we hypothesize that FGFR1 may regulate NF $\kappa$ B activation through MAPKs in cardiomyocytes. Firstly, we found increased levels of phosphorylated ERK, JNK, and p38 in H9C2 cells exposed to HG (Fig. 4F, Supporting Information Fig. S12A). However, these increases were not seen in cells following FGFR1 knockdown. Similar results were obtained when rat primary cardiomyocytes

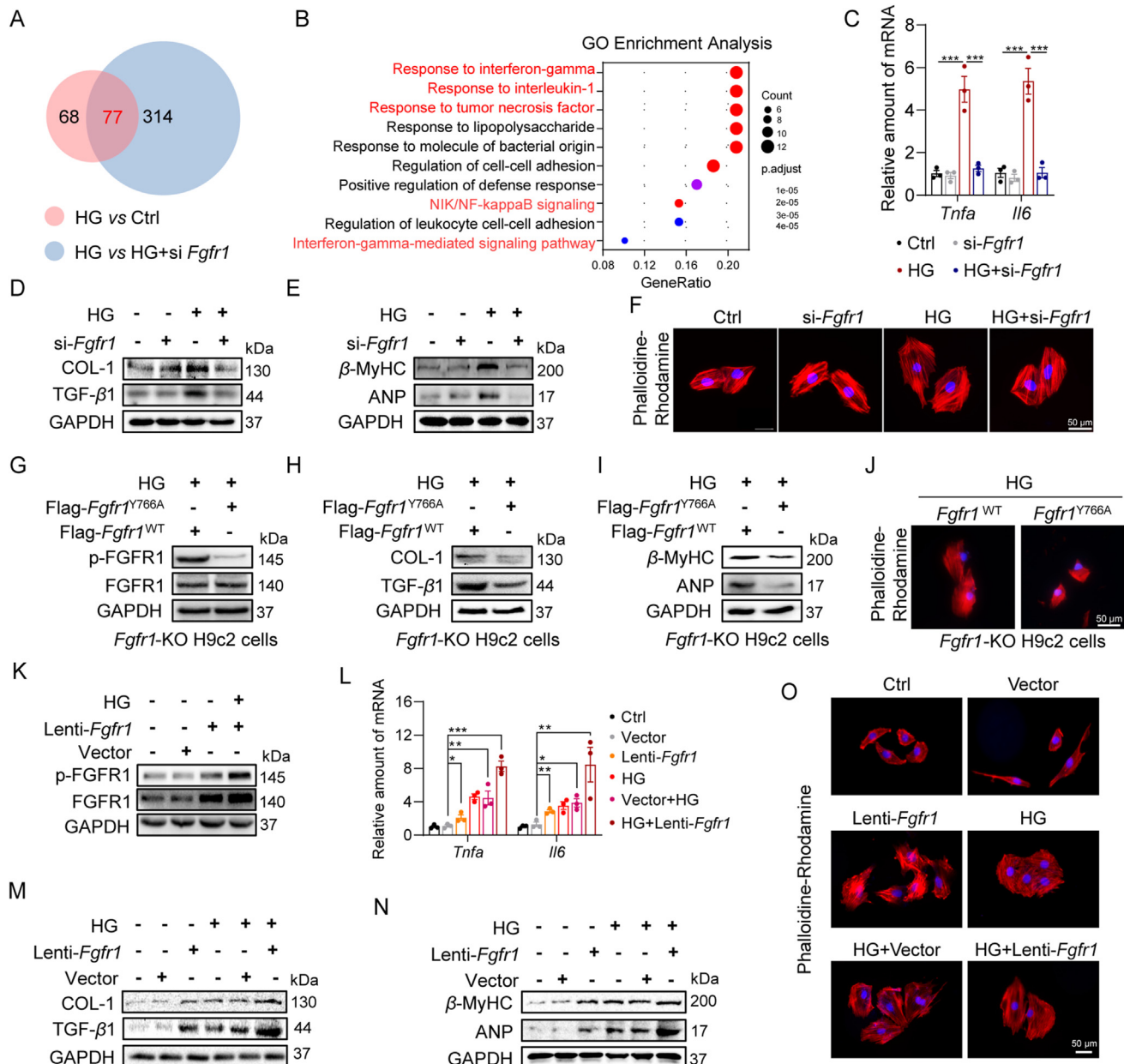


**Figure 3** HG-induced FGFR1 activation leads to inflammatory injuries in cardiomyocytes. (A) Venn diagram of differentially expressed genes in H9C2 cells. H9C2 cells were transfected with or without FGFR1 siRNA. Cells were then exposed to HG for 8 h. RNA from Ctrl, HG, and HG + siFGFR1 ( $n = 3$ ) was sequenced. (B) GO analysis showing FGFR1 regulated inflammatory response genes in H9C2 cells. The inflammation-related pathways were highlighted in red font. (C) mRNA levels of TNF- $\alpha$  and IL-6 in H9C2 cells exposed to HG for 6 h (mean  $\pm$  SEM,  $n = 3$ ;  $***P < 0.001$ ). (D, E) H9C2 cells were transfected with FGFR1 siRNA and exposed to HG for 24 h. Lysates were probed for COL-1 (D), TGF $\beta$ 1 (D),  $\beta$ -MyHC (E), and ANP (E). GAPDH was used as loading control. (F) Rhodamine phalloidin staining of H9C2 cells, showing the effects of HG following FGFR1 knockdown. Cells were counterstained with DAPI (blue) (Scale bar = 50  $\mu$ m). (G) FGFR1-deleted (*Fgfr1*-KO) H9C2 cells were transfected with Flag-*Fgfr1*<sup>Y766A</sup> or Flag-*Fgfr1*<sup>WT</sup>. Cells were then exposed to HG for 15 min. Levels of p-FGFR1 and His-tag were measured by immunoblotting. (H, I) *Fgfr1*-KO H9C2 cells were prepared as in Panel (G) but exposed to HG for 24 h. Lysates from cells were probed for COL-1 (H), TGF $\beta$ 1 (H),  $\beta$ -MyHC (I), and ANP (I). (J) Rhodamine phalloidin staining of *Fgfr1*-KO H9C2 cells. Cells were prepared and treated as in Panel (H) (Scale bar = 50  $\mu$ m). (K) H9C2 cells were transfected with full-length FGFR1 (Lenti-*Fgfr1*) or empty vector (NC). Cells were then exposed to HG for 15 min. Levels of p-FGFR1 (Tyr 766) were measured by immunoblotting. Total FGFR1 and GAPDH were used as controls. (L) mRNA levels of TNF- $\alpha$  and IL-6 in H9C2 cells exposed to HG for 6 h (mean  $\pm$  SEM,  $n = 3$ ;  $*P < 0.05$ ,  $**P < 0.01$ ,  $***P < 0.005$ ). (M, N) H9C2 cells were prepared as in Panel (K) but exposed to HG for 24 h. Lysates from cells were probed for COL-1 (M), TGF- $\beta$ 1 (M),  $\beta$ -MyHC (N), and ANP (N). (O) Rhodamine phalloidin staining of H9C2 cells. Treatment of cells was carried out as in Panel (M) (Scale bar = 50  $\mu$ m).

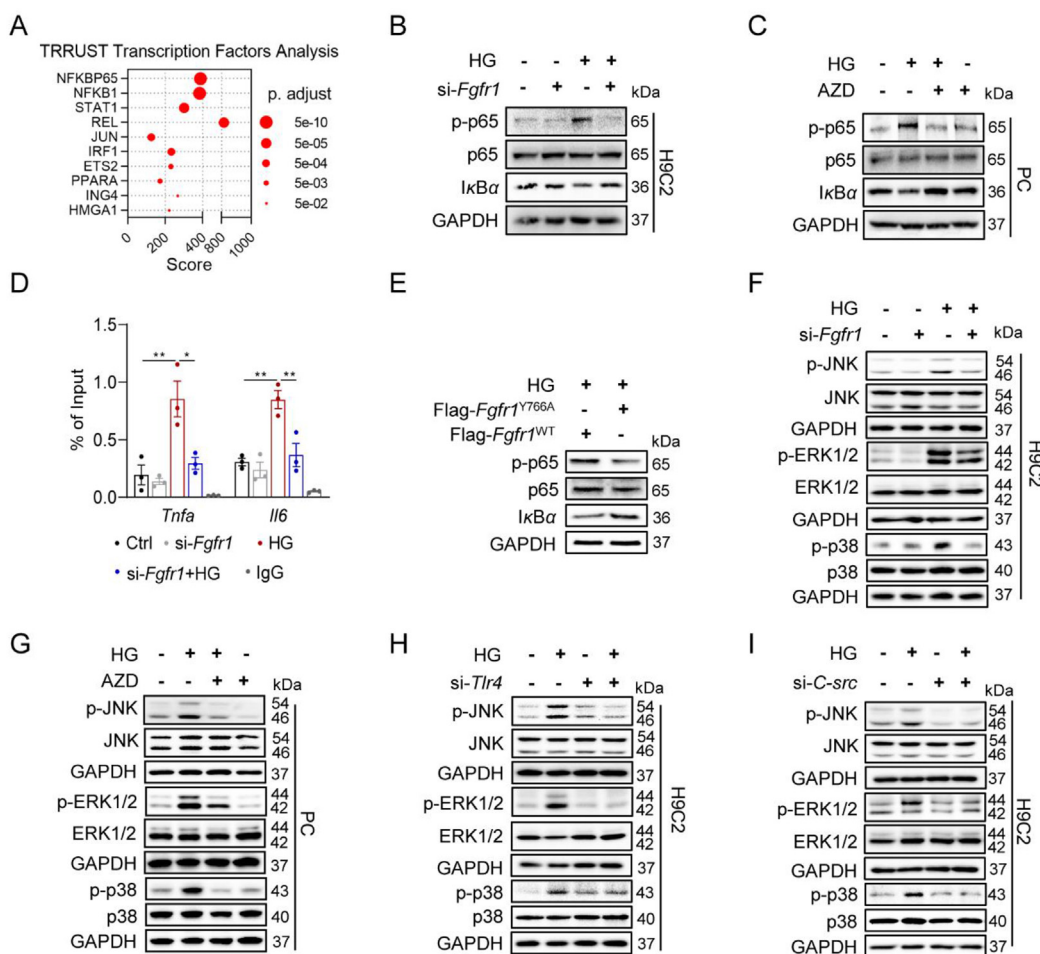


**Figure 4** NF $\kappa$ B links FGFR1 to downstream responses in HG-exposed cardiomyocytes. (A) TRRUST Transcription Factors analysis showing the top 10 protein-coding transcripts (ranked by adjusted *P*-value) that were increased by HG and suppressed by FGFR1 knockdown. (B) Immunoblot analysis of p-p65, p65, and I $\kappa$ B $\alpha$  in H9C2 cells. Cells were transfected with FGFR1 siRNA and then exposed to HG for 30 min. GAPDH was used as control. (C) Rat primary cardiomyocytes were pretreated with 5  $\mu$ mol/L AZD4547 for 1 h and then exposed to 33 mmol/L HG for 30 min. Levels of p-p65, p65, and I $\kappa$ B $\alpha$  were measured, with GAPDH as control. (D) H9C2 cells were transfected with FGFR1 siRNA and then exposed to HG for 8 h. NF $\kappa$ B p65 antibody was used for ChIP. Candidate gene promoters (*Tnfa* and *Il6*) were detected by qPCR (mean  $\pm$  SEM, *n* = 3; \**P* < 0.05; \*\**P* < 0.01). (E) *Fgfr1*-KO H9C2 cells were transfected with Flag-*Fgfr1*<sup>Y766A</sup> or Flag-*Fgfr1*<sup>WT</sup>. Cells were then exposed to HG for 30 min. Levels of p-p65, p65, and I $\kappa$ B $\alpha$  were measured by immunoblotting with GAPDH as loading control. (F) H9c2 cells were prepared and treated as indicated in Panel (B). Levels of p-ERK1/2, p-JNK, and p-p38 were measured. Total proteins and GAPDH were used as controls. (G) Rat primary cardiomyocytes were pretreated with 5  $\mu$ mol/L AZD4547 for 1 h and then exposed to 33 mmol/L HG for 30 min. Levels of p-ERK1/2, p-JNK, and p-p38 were measured. Total proteins and GAPDH were used as controls. (H, I) H9C2 cells were transfected with TLR4 siRNA (H) or c-Src siRNA (I) and then exposed to HG for 30 min. Lysates were probed for levels of phosphorylated MAPK pathway proteins. Total proteins and GAPDH were used as controls.

(Fig. 4G, Fig. S12B) and H9C2 cells (Fig. S12C) were treated with FGFR1 inhibitor AZD before HG exposure. Furthermore, knocking down the upstream TLR4 or c-Src also prevented HG-induced MAPKs activation in H9C2 cells (Fig. 4H and I, Fig. S12D and S12E). Selective inhibition of individual MAPKs signaling arms showed that these proteins are involved in HG-induced NF $\kappa$ B activation (Fig. S12F) and downstream gene expression (Fig. S12G). These results show that HG activates FGFR1 to lead to MAPKs and NF $\kappa$ B activation, triggering the expression of pro-inflammatory and deleterious target genes in cardiomyocytes.

### 3.5. Cardiomyocyte-specific FGFR1 deficiency protects against diabetes-induced cardiac injury

Tamoxifen-inducible cardiomyocyte-specific FGFR1 knockout mice were generated for *in vivo* studies (Fig. S7A and S7B). We first examined the possible effect of cardiomyocyte-specific FGFR1-knockout on the baseline of heart structure and function using the *Fgfr1*<sup>fllox</sup> and *Fgfr1*<sup>ΔCM</sup> mice without diabetes. As shown in Supporting Information Fig. S13A–S13L and Table S6, there are no significant differences in blood glucose level, body weight gain, cardiac structure, function, pathophysiologic phenotypes,

and inflammatory markers between *Fgfr1<sup>fllox</sup>* mice and *Fgfr1<sup>ΔCM</sup>* mice without diabetes. These data indicate that, during the 32-week experiment, FGFR1 deficiency in cardiomyocytes did not affect the baseline of adult mouse hearts.

Afterward, *Fgfr1<sup>fllox</sup>* and *Fgfr1<sup>ΔCM</sup>* mice were made diabetic by multiple-low dose STZ injections. Analysis of blood glucose and body weight gain showed no difference between diabetic *Fgfr1<sup>fllox</sup>* mice and *Fgfr1<sup>ΔCM</sup>* mice (Fig. 5A and B). However, cardiac functional parameters, including systolic and diastolic function measured by echocardiography, showed that cardiomyocyte

FGFR1 knockout mice exhibit preserved cardiac function (Fig. 5C, Table 1). Despite of the relatively high EF values in all mice, which may result from the differences in echocardiography equipment and readout, our data showed that FGFR1 deficiency significantly reversed diabetes-decreased EF values in diabetic mice. In agreement with the changes in cardiac function, serum levels of cardiac injury markers, B-type natriuretic peptide (BNP), creatine kinase-MB (CK-MB), and lactate dehydrogenase (LDH) were all elevated in diabetic *Fgfr1<sup>fllox</sup>* mice but not in diabetic *Fgfr1<sup>ΔCM</sup>* mice (Fig. 5D and E). Harvested heart tissues were then

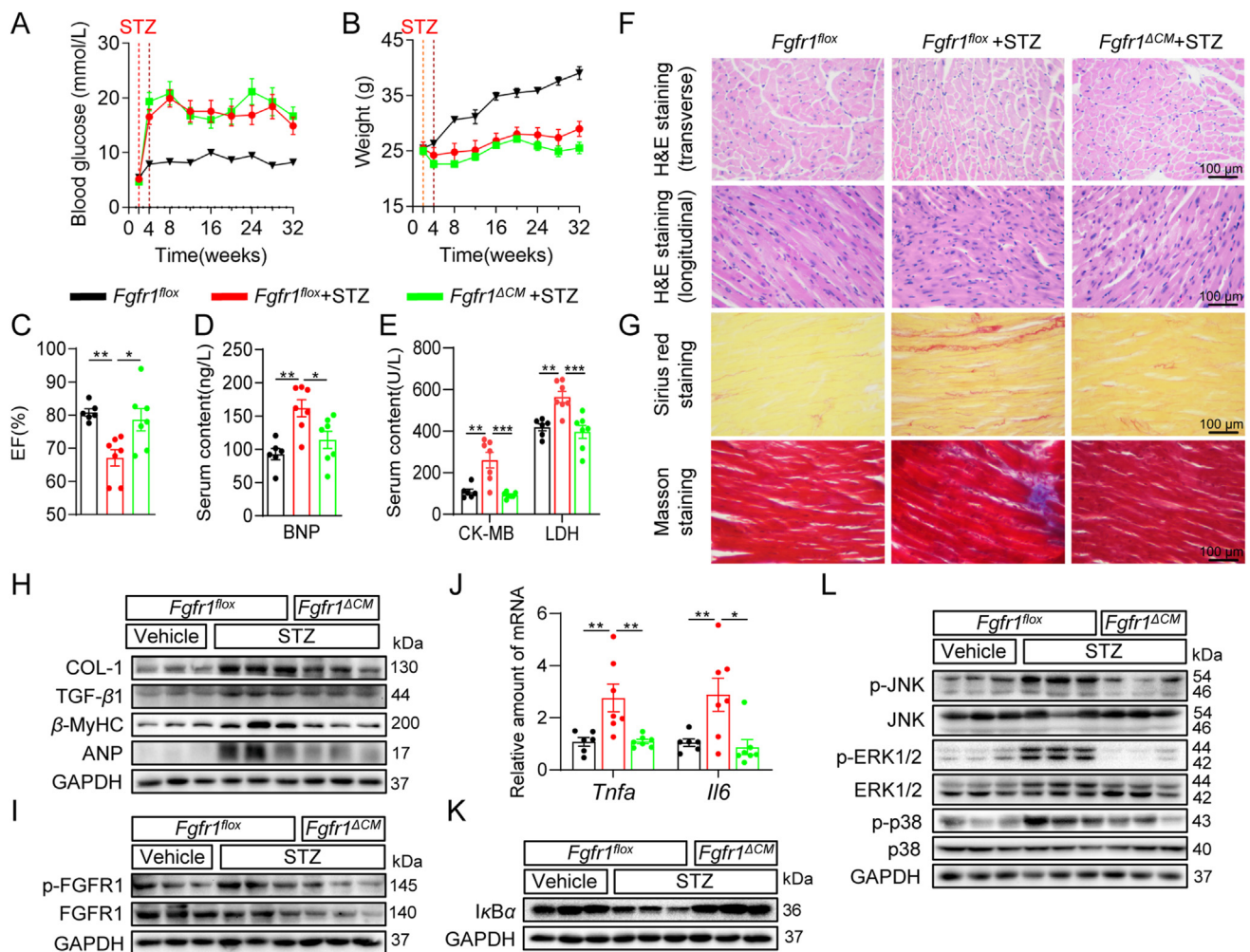


**Figure 5** Cardiac-specific FGFR1 deficiency protects hearts in STZ-induced diabetic mice. Diabetes was induced in *Fgfr1<sup>fllox</sup>* and *Fgfr1<sup>ΔCM</sup>* mice by STZ injection. Heart tissues were harvested 28 weeks following the onset of diabetes (*Fgfr1<sup>fllox</sup>*,  $n = 6$ ; *Fgfr1<sup>fllox</sup>* + STZ,  $n = 7$ , *Fgfr1<sup>ΔCM</sup>* + STZ,  $n = 7$ ). (A, B) Mice were followed up with weekly measurements of blood glucose (A) and body weights (B). (C) Ejection fraction values from the transthoracic echocardiography of the mice (mean  $\pm$  SEM,  $n = 6$ –7; \* $P < 0.05$ , \*\* $P < 0.01$ ). (D, E) Levels of B-type natriuretic peptide (BNP; D), creatine kinase-MB (heart muscle isoform; E), and lactate dehydrogenase (LDH; E) in the blood of mice at the conclusion of the study (mean  $\pm$  SEM,  $n = 6$ –7; \* $P < 0.05$ , \*\* $P < 0.01$ , \*\*\* $P < 0.001$ ). (F) Longitudinal and transversal H&E-stained sections of mouse hearts. (G) Mouse heart sections were stained with Sirius Red (upper panel) and Masson’s Trichrome stain (lower panel) to assess fibrotic changes. (H) Immunoblot analysis of COL-1, TGF- $\beta$ 1,  $\beta$ -MyHC, and ANP in heart tissues of mice, with GAPDH as a loading control. (I) Levels of p-FGFR1 and FGFR1 in heart tissue lysates. GAPDH was used as control. (J) mRNA levels of TNF- $\alpha$  and IL-6 in heart tissues by real-time qPCR assay (mean  $\pm$  SEM,  $n = 6$ –7; \* $P < 0.05$ , \*\* $P < 0.01$ ). (K) Immunoblot analysis of I $\kappa$ B $\alpha$  in heart tissue lysates. GAPDH was used as control. GAPDH was used as control. (L) Activation of the MAPK pathway was assessed by probing for phosphorylated JNK, ERK, and p38. Total proteins and GAPDH were used as controls.

**Table 1** Cardiac function parameters in STZ-induced diabetic mice with or without cardiomyocyte FGFR1 knockout.

Cardiac function	<i>Fgfr1<sup>fllox</sup></i> (n = 6)	STZ	
		<i>Fgfr1<sup>fllox</sup></i> (n = 7)	<i>Fgfr1<sup>ΔCM</sup></i> (n = 7)
EF (%)	80.79 ± 1.08	67.11 ± 2.49**	78.62 ± 3.35 <sup>#</sup>
FS (%)	43.26 ± 1.12	29.84 ± 2.10*	38.2 ± 2.12 <sup>#</sup>
LVIDd (mm)	2.70 ± 0.09	3.13 ± 0.08**	2.79 ± 0.07 <sup>#</sup>
IVSd (mm)	0.75 ± 0.02	0.76 ± 0.02	0.69 ± 0.03
LVAWd (mm)	0.68 ± 0.02	0.73 ± 0.02	0.67 ± 0.03
LVPWd (mm)	0.70 ± 0.03	0.74 ± 0.02	0.66 ± 0.02 <sup>#</sup>
IRT (ms)	15.50 ± 1.41	17 ± 0.44	18.29 ± 0.84
Tei index	0.81 ± 0.09	1.09 ± 0.09*	0.77 ± 0.03 <sup>#</sup>
Heart rate (bpm)	535 ± 45	565 ± 7	480 ± 16

STZ, streptozotocin-induced diabetic; EF, ejection fraction; FS, fractional shortening; LVIDd, diastole left ventricle internal dimension; IVSd, diastole interventricular septal thickness; LVAWd, left ventricular anterior wall thickness in diastole; LVPWd, left ventricle posterior wall thickness in diastole; IRT, isovolumic relaxation time; Tei index, myocardial performance index.

Data are mean ± SEM; n = 6 or 7; \**P* < 0.05, \*\**P* < 0.01 compared to *Fgfr1<sup>fllox</sup>*; <sup>#</sup>*P* < 0.05 compared to STZ + *Fgfr1<sup>fllox</sup>*.

stained for histological analyses. The H&E staining of transverse sections mainly indicated that cardiomyocyte FGFR1 knockout prevented the levels of cardiomyocyte hypertrophy in diabetic mice. H&E staining of longitudinal sections reflected the structural abnormalities, broken fibers, and deranged cellular structures in diabetic *Fgfr1<sup>fllox</sup>* mouse hearts, while these pathological changes were not observed in *Fgfr1<sup>ΔCM</sup>* mice (Fig. 5F, Supporting Information Fig. S14A). Staining of heart tissues with Sirius Red and Masson's Trichrome also showed that FGFR1 knockout mice are protected against diabetes-induced cardiac fibrosis (Fig. 5G, Fig. S14B). We then prepared lysates from heart tissues and showed that FGFR1 knockout reversed the increased protein levels of COL-1, TGF-β1, ANP, and β-MyHC in diabetic mice (Fig. 5H, Fig. S14C). mRNA levels of these genes showed the same pattern (Fig. S14D). These results suggest that cardiomyocyte-specific FGFR1 affords cardiac protection in diabetes.

We also examined the FGFR1-MAPKs/NFκB inflammatory signaling pathway in mouse hearts. Cardiomyocyte FGFR1 knockout reduced FGFR1 expression and phosphorylation in lysates from diabetic heart tissues (Fig. 5I, Fig. S14E). FGFR1 knockout mice do not exhibit increases in inflammatory genes including *Tnfa*, *Il6*, *Il1b*, *Il18*, *Icam1*, *Vcam1*, and *Ccl2* upon diabetes induction (Fig. 5J, Fig. S14F). Moreover, cardiomyocyte-specific FGFR1 deletion reduced CD68 levels in diabetic heart tissues, indicating suppressed macrophage infiltration (Fig. S14G). Consistent with our *in vitro* findings, activation of NFκB and MAPKs in diabetic mouse hearts was significantly prevented by FGFR1 knockout (Fig. 5K and L, and Fig. S14H and S14I). These studies associate inflammatory diabetic cardiomyopathy to cardiomyocyte-specific FGFR1 activation.

### 3.6. Pharmacological inhibition of FGFR1 protects mice against DCM

Our next objective was to utilize the selective FGFR1 inhibitor AZD4547 and determine whether it is effective in treating DCM. We made type 1 diabetic mice by STZ injection and initiated regular AZD administration. After 20 weeks of diabetes duration, we performed similar studies as with the conditional FGFR1 knockout mice. As expected, the FGFR1 inhibitor did not alter blood glucose levels or impaired weight gain in diabetic mice

(Fig. 6A and B). Echocardiography assay showed that FGFR1 inhibitor protected heart systolic and diastolic function in diabetic mice (Fig. 6C, Table 2). Cardiac biomarkers in the serum showed that FGFR1 inhibitor reduced cardiac injury in diabetic mice (Fig. 6D and E). Histological analysis of heart tissues, including H&E staining, Sirius Red, and Masson Trichrome staining, showed that AZD4547 is effective in reducing structural alterations and fibrosis in heart tissues of diabetic mice (Fig. 6F and G, Supporting Information Fig. S15A and S15B). Furthermore, protein levels of fibrosis- and hypertrophy-associated factors showed a lack of induction when diabetic mice were treated with AZD4547 (Fig. 6H, Fig. S15C). Finally, we measured the FGFR1-MAPK/NFκB signaling pathway in heart tissues, including FGFR1 phosphorylation, mRNA levels of inflammatory genes, CD68 level, NFκB activation, and MAPK phosphorylation. In all assays, diabetes-induced increases/activation were prevented by AZD4547 treatment (Fig. 6I–L, Fig. S15D–S15H).

Considering that the majority of DCM cases are secondary to type 2 diabetes, we examine the cardioprotective effects of FGFR1 inhibition in *db/db* type 2 diabetic mice. As expected, AZD4547 treatment did not alter blood glucose levels or weight gain in *db/db* mice (Fig. 7A and B). Consistent with the results in type 2 diabetic model, FGFR1 inhibitor AZD4547 also significantly prevents cardiac dysfunction, pathological changes, fibrosis, hypertrophy, and inflammation in *db/db* type 2 diabetic mice, accompanied with MAPKs/NFκB inactivation in heart tissue (Fig. 7C–L, Fig. S16A–S16I, Table 3). Collectively, these data show that pharmacological inhibition of FGFR1 by AZD4547 affords efficient protection against inflammatory DCM in both type 1 and type 2 diabetic mice.

## 4. Discussion

In the present study, we profiled RTK phosphorylation and found increased activating FGFR1 phosphorylation levels in cardiomyocytes of diabetic mice. FGFR1 signaling is usually mitogenic. Here, we discovered a novel, yet critical role of FGFR1 in diabetic cardiomyopathy. We found that HG phosphorylates FGFR1 through TLR4 and c-Src, rather than GLUT1/4 and FGF ligands. HG-induced FGFR1 activation induces inflammatory responses through activating MAPK/NFκB, which further

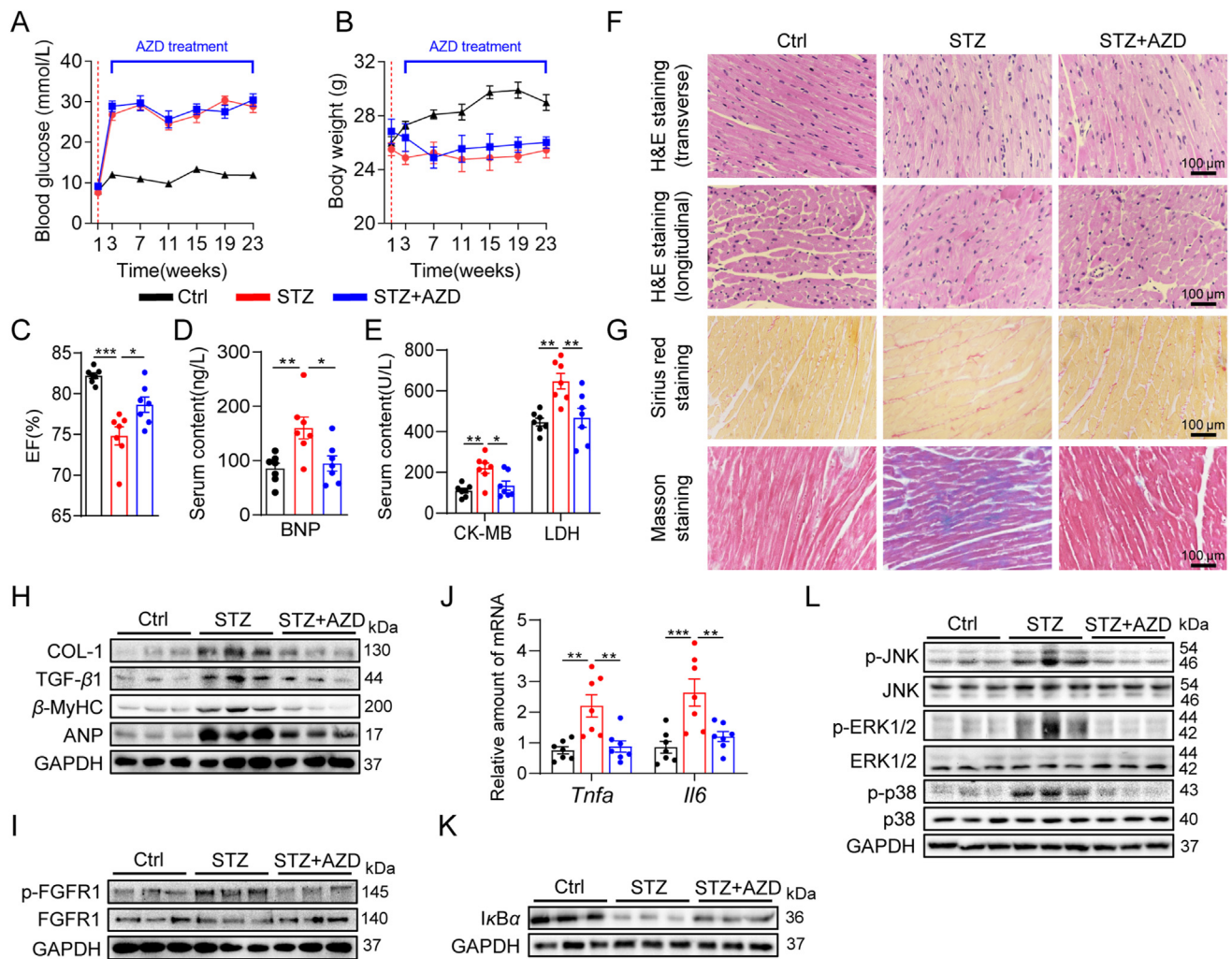


**Figure 6** Inhibition of FGFR1 by AZD4547 prevents cardiac injury in STZ-induced diabetic mice. Mice were made diabetic with STZ. FGFR1 was inhibited by treating mice with 5 mg/kg AZD4547 every other day. Heart tissues were examined at week 20 following the onset of diabetes (Ctrl, control group; STZ, type one diabetic group; STZ + AZD, AZD4547-treated diabetic group;  $n = 7$  per group). (A, B) Weekly measurements showing levels of blood glucose (A) and body weights (B) in mice. (C) Ejection fraction values from the transthoracic echocardiography of the mice (mean  $\pm$  SEM,  $n = 7$ ;  $*P < 0.05$ ,  $***P < 0.001$ ). (D, E) Levels of BNP (D), CK-MB (E), and LDH (E) in blood samples of mice at the conclusion of the study (mean  $\pm$  SEM,  $n = 7$ ;  $*P < 0.05$ ,  $***P < 0.01$ ). (F) Longitudinal and transversal H&E-stained sections of mouse hearts. (G) Heart sections were stained with Sirius Red (upper panel) and Masson's Trichrome stain (lower panel) to assess fibrotic changes. (H) Levels of COL-1, TGF- $\beta$ 1,  $\beta$ -MyHC, and ANP proteins in the heart tissues of mice were detected by immunoblotting. GAPDH was used as control. (I) Levels of pFGFR1 and FGFR1 in heart tissue lysates. GAPDH was used as control. (J) mRNA levels of TNF- $\alpha$  and IL-6 in heart tissues of mice (mean  $\pm$  SEM,  $n = 7$ ;  $**P < 0.01$ ,  $***P < 0.001$ ). (K) Levels of I $\kappa$ B $\alpha$  in heart tissue lysates. GAPDH was used as control. (L) MAPK pathway activation was determined by measuring levels of p-JNK, p-ERK, and p-p38. Total proteins and GAPDH were used as controls.

results in fibrosis and hypertrophy in cardiomyocytes. Either cardiomyocyte-specific FGFR1 knockout or selective FGFR1 inhibitor prevents diabetes-induced inflammation, fibrosis, and hypertrophy, leading to preserved cardiac function in both type 1 and type 2 diabetic mice. A schematic illustration of the main findings is shown in Fig. 8.

The involvement of FGFR1 in diabetic cardiomyopathy was an interesting finding. FGFR1 is expressed in the mouse heart<sup>39</sup>, and immunohistochemical staining of normal human tissues also

reveals robust expression of FGFR1 in cardiomyocytes<sup>40</sup>. The involvement of FGFR1 was, however, surprising because our previous studies have examined the effect of FGF ligand administration in diabetic models with contrasting results<sup>41</sup>. Specifically, we showed that chronic administration of FGF1 to STZ-induced and *db/db* diabetic mice significantly suppresses renal inflammation, glomerular and tubular damage, and renal dysfunction. In this experimental setting, FGF1 administration would be expected to activate FGFRs. There are two possible explanations for the

**Table 2** Cardiac function parameters in STZ induced-diabetic mice with or without AZD4547 treatment.

Cardiac function	Ctrl ( <i>n</i> = 7)	STZ	
		Vehicle ( <i>n</i> = 7)	AZD4547 ( <i>n</i> = 7)
EF (%)	82.23 ± 0.34	74.83 ± 1.11***	78.66 ± 0.93 <sup>#</sup>
FS (%)	44.59 ± 0.34	37.70 ± 0.91***	41.21 ± 0.94 <sup>#</sup>
LVIDd (mm)	2.30 ± 0.03	2.63 ± 0.06***	2.43 ± 0.04 <sup>#</sup>
IVSd (mm)	0.76 ± 0.01	0.80 ± 0.01*	0.75 ± 0.01 <sup>#</sup>
LVAWd (mm)	0.75 ± 0.01	0.79 ± 0.01**	0.75 ± 0.01 <sup>##</sup>
LVPWd (mm)	0.77 ± 0.01	0.80 ± 0.01*	0.75 ± 0.01 <sup>##</sup>
IRT (ms)	15.57 ± 1.02	26.57 ± 3.51*	22.43 ± 1.95
Tei index	0.67 ± 0.03	0.95 ± 0.05***	0.75 ± 0.03 <sup>##</sup>
Heart rate (bpm)	434 ± 8	473 ± 19	450 ± 22

Ctrl, non-diabetic control mice; STZ, streptozotocin-induced diabetic; AZD, mice treated with AZD4547; EF, ejection fraction; FS, fractional shortening; LVIDd, diastole left ventricle internal dimension; IVSd, diastole interventricular septal thickness; LVAWd, left ventricular anterior wall thickness in diastole; LVPWd, left ventricle posterior wall thickness in diastole; IRT, isovolumic relaxation time; Tei index, myocardial performance index.

Data are mean ± SEM; *n* = 7; \**P* < 0.05, \*\*\**P* < 0.01 compared to Ctrl; <sup>#</sup>*P* < 0.05, <sup>##</sup>*P* < 0.01 compared to STZ.

difference in results. First, some of the beneficial effects of FGF treatment may be independent of FGFR1. Support for this possibility comes from studies that have utilized mutant FGF ligands. Huang and colleagues<sup>42</sup> engineered FGF1 mutants, termed FGF1ΔHBS, that exhibit reduced ability to activate FGFR. In a mouse model of chronic kidney disease, treatment with FGF1ΔHBS reduced inflammation and oxidative stress<sup>43</sup>. Similarly, FGF1ΔHBS prevented diabetes-induced cardiac injury and remodeling<sup>44</sup>.

Another possible explanation of the beneficial effects seen in models of FGF ligand supplementation is related to disease context. From our present study and the previous one<sup>41</sup>, diabetes either suppresses or fails to change the levels of FGF ligands. In this context, restoration of FGF ligands or administration of exogenous factors possibly tips the balance towards the well-known and protective role of FGFR1 activity. In support of this notion, studies have shown that FGF1, together with TNF-related weak inducer of apoptosis (TWEAK), binds to FGFR1 and induces cardiomyocyte cycle re-entry<sup>45</sup>. Therefore, context becomes critical. There is sufficient evidence that FGFR can be subverted to positively contribute to disease progression. Cardiomyocyte-specific overexpression of constitutively active FGFR1 (deleterious activity) in mice has been shown to increase cardiac contractility and result in hypertrophic cardiomyopathy<sup>46</sup>. Histological analysis also showed increased cardiac fibrosis. In other disease models as well, activation of the FGFR1 kinase increased inflammation and drove prostate cancer progression<sup>47</sup>.

There are a handful of studies, mostly quite recent, that have shown a cause-and-effect relationship between tyrosine kinase inhibitors and diabetic injuries, including those in the heart. Chronic administration of selective EGFR inhibitor AG1478 and ErbB2 inhibitor AG825 decreased cardiac recovery in normal and diabetic rats<sup>48</sup>. Whereas administration of the EGFR ligand, EGF, led to an improvement in cardiac recovery. In contrast, Galan and colleagues<sup>13</sup> showed that EGFR phosphorylation was increased in the heart of STZ-induced diabetic mice and associated with cardiac fibrosis. A limitation of both aforementioned studies is a lack of detailed histopathological assessment in these models. In one of our previous studies<sup>14</sup>, we added this missing dimension. We showed that EGFR inhibitors protected against

diabetes-induced cardiac damage and remodeling<sup>49</sup>. Our present study, identifying FGFR1 activation, has added to this growing knowledge base on tyrosine kinases and the pathogenesis of diabetic cardiomyopathy.

Interestingly, the RTK phosphorylation profile provides us with new information on the changing form of RTKs under diseases. We identified an increase in FGFR1 phosphorylation, but no change in FGFR1 expression level, in diabetic hearts. In addition, HG challenge induced FGFR1 phosphorylation, rather than FGFR1 overexpression, in cultured cardiomyocytes. This trend is consistent with the change of p-EGFR/EGFR in DCM<sup>14</sup>. We found that deletion of FGFR1 protects hearts against diabetes/HG-induced injuries by reducing the level of FGFR1 phosphorylation. We also validated the role of FGFR1 phosphorylation by using the *Fgfr1* Y766A mutation in cardiomyocytes. It may explain why the identification of non-tumoral roles of RTKs, including FGFR1, is lagging since most of the screening techniques rely on transcript level and sequencing. Ideally, of course, coupling gene-level alterations with phosphorylation-based activation would provide a thorough and therapeutically applicable understanding of functional proteins in diseases.

The overlap between the downstream endpoints of increased FGFR1 activity in the heart (present study) and previous reports on EGFR<sup>13,14</sup> suggest a common activation mechanism of these two receptor tyrosine kinases. Our studies highlight the critical role of TLR4/c-Src in mediating FGFR1 activation. We previously showed that HG causes rapid activation of TLR4 through a co-receptor called myeloid differentiation factor 2 (MD2)<sup>25</sup>. Could it be possible that EGFR is also activated through a similar, TLR4-mediated mechanism? There is direct evidence to support this notion. Almost simultaneously, two separate research groups found that LPS transactivated EGFR through TLR4 and c-Src to mediate inflammatory responses in macrophages and septic mouse models<sup>30,31</sup>. More interestingly, tyrosine-phosphorylated TLR4 interacted with EGFR and this interaction was necessary for the activation of EGFR<sup>50</sup>. These studies facilitate the interaction between TLR4 and receptor tyrosine kinases, including EGFR and FGFR.

Our study reveals that deficiency in FGFR1 activity, though cardiomyocyte-specific deletion or systemic FGFR1 inhibitor

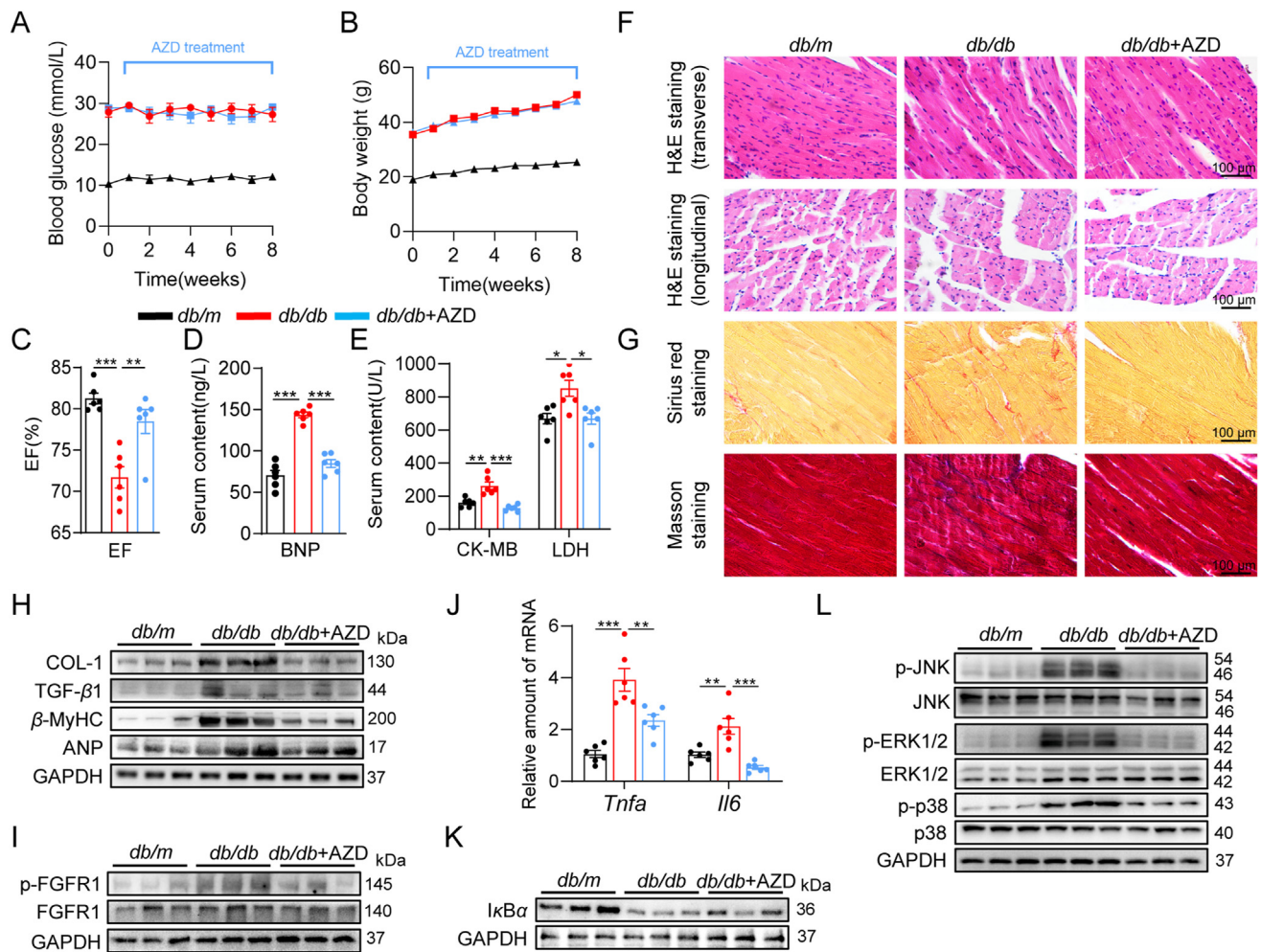


**Figure 7** Inhibition of FGFR1 by AZD4547 prevents cardiac injury in *db/db* mice. FGFR1 was inhibited by treating *db/db* mice with 5 mg/kg AZD4547 every other day. Heart tissues were examined at Week 8 following AZD4547 treatment (*db/m*, control group; *db/db*, type 2 diabetic group; *db/db* + AZD, AZD4547-treated diabetic group;  $n = 6$  per group). (A, B) Weekly measurements showing levels of blood glucose (A) and body weights (B) in mice. (C) Ejection fraction values from the transthoracic echocardiography of the mice (mean  $\pm$  SEM,  $n = 6$ ;  $**P < 0.01$ ,  $***P < 0.001$ ). (D, E) Levels of BNP (D), CK-MB (E), and LDH (E) in blood samples of mice at the conclusion of the study (mean  $\pm$  SEM,  $n = 6$ ;  $*P < 0.05$ ,  $**P < 0.01$ ,  $***P < 0.001$ ). (F) Longitudinal and transversal H&E-stained sections of mouse hearts. (G) Heart sections were stained with Sirius Red (upper panel) and Masson's Trichrome stain (lower panel) to assess fibrotic changes. (H) Levels of COL-1, TGF- $\beta$ 1,  $\beta$ -MyHC, and ANP proteins in the heart tissues of mice were detected by immunoblotting. GAPDH was used as control. (I) Levels of pFGFR1 and FGFR1 in heart tissue lysates. GAPDH was used as control. (J) mRNA levels of TNF- $\alpha$  and IL-6 in heart tissues of mice (mean  $\pm$  SEM,  $n = 6$ ;  $**P < 0.01$ ,  $***P < 0.001$ ). (K) Levels of I $\kappa$ B $\alpha$  in heart tissue lysates. GAPDH was used as control. (L) MAPK pathway activation was determined by measuring levels of p-JNK, p-ERK, and p-p38. Total proteins and GAPDH were used as controls.

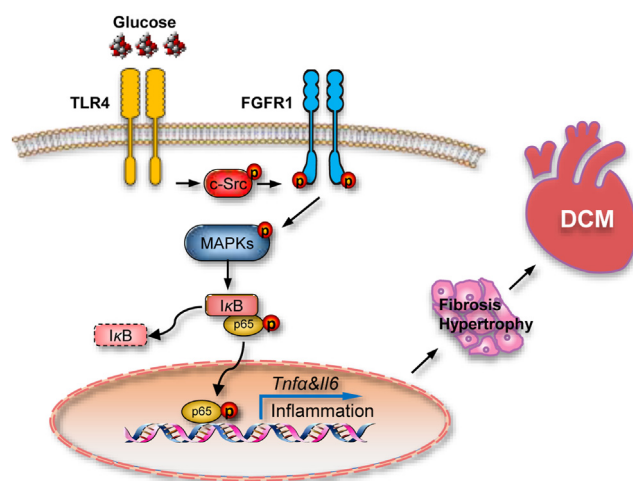
administration, is associated with suppression of both pro-inflammatory responses and related subsequent injuries to the heart. Myocardial inflammation is deemed important in diabetic cardiomyopathy development<sup>51,52</sup>. It is believed that these pro-inflammatory factors cause heart wall stiffening and decreased contractility<sup>53,54</sup>. There is strong evidence that NF $\kappa$ B activation contributes to cardiac inflammation, myocardial fibrosis, hypertrophy, apoptosis, and ventricular dysfunction<sup>55,56</sup>. Partly based on these studies, antagonism or suppression of

pro-inflammatory cytokines has been proposed as an approach to deal with diabetic cardiomyopathy. Our RNA-seq results indicated NF $\kappa$ B as a downstream transcriptional factor of FGFR1 activation in cardiomyocytes. Subsequent experiments validated the FGFR1–MAPKs–NF $\kappa$ B signaling axis in HG-challenged cardiomyocytes and diabetic hearts. Based on our studies, it is prudent that we explore targeting FGFR1, TLR4, and NF $\kappa$ B to see if we can combat diabetic cardiomyopathy.

**Table 3** Cardiac function parameters in *db/db* mice with or without AZD4547 treatment.

Cardiac function	<i>db/m</i> (n = 6)	<i>db/db</i>	
		Vehicle (n = 6)	AZD (n = 6)
EF (%)	81.26 ± 0.66	71.72 ± 1.30***	78.48 ± 1.45##
FS (%)	43.71 ± 0.71	35.30 ± 1.02***	40.99 ± 1.28##
LVIDd (mm)	2.82 ± 0.18	3.01 ± 0.14*	2.52 ± 0.10
IVSd (mm)	0.72 ± 0.02	0.82 ± 0.02**	0.73 ± 0.05##
LVAWd (mm)	0.65 ± 0.02	0.82 ± 0.02***	0.72 ± 0.03#
LVPWd (mm)	0.67 ± 0.02	0.82 ± 0.03**	0.72 ± 0.02#
IRT (ms)	14.67 ± 0.61	18.83 ± 0.83***	16.17 ± 0.40#
Tei index	0.63 ± 0.03	0.82 ± 0.06*	0.67 ± 0.03#
Heart rate (bpm)	539 ± 10	510 ± 20	531 ± 9

*db/m*, non-diabetic control mice; *db/db*, *db/db* diabetic mice; AZD, mice treated with AZD4547; EF, ejection fraction; FS, fractional shortening; LVIDd, diastole left ventricle internal dimension; IVSd, diastole interventricular septal thickness; LVAWd, left ventricular anterior wall thickness in diastole; LVPWd, left ventricle posterior wall thickness in diastole; IRT, isovolumic relaxation time; Tei index, myocardial performance index. Data are mean ± SEM; n = 6; \*P < 0.05, \*\*P < 0.05, \*\*\*P < 0.01 compared to *db/m*; #P < 0.05, ##P < 0.01 compared to *db/db*.

**Figure 8** The role of FGFR1 in diabetic cardiomyopathy.

## 5. Conclusions

We have provided, to the best of our knowledge, the first empirical evidence showing increased FGFR1 phosphorylation and activity in diabetic cardiomyopathy. We show that HG-induced FGFR1 activation is mediated through TLR4 and c-Src in cardiomyopathy, which converges on MAPKs-mediated NFκB activation to increase the transcription of inflammatory cytokines and subsequent fibrosis and hypertrophy. Mice lacking FGFR1 in cardiomyocytes fail to show the well-established structural alterations of excessive cardiac remodeling and functional deficits upon diabetes induction. Pharmacological FGFR1 inhibition also protects hearts in both type 1 and type 2 diabetic mice. A limitation is that we have not examined FGFR1 activation in human hearts, since it is very difficult to get human heart samples from diabetic subjects. Nonetheless, these studies have advanced our understanding of diabetic cardiomyopathy and suggest developing FGFR1 as a target for the treatment of cardiomyopathy.

## Acknowledgments

This study was supported by the National Key Research Project (2017YFA0506000 to Guang Liang, China), and National Natural

Science Foundation of China (81930108 to Guang Liang and 82000793 to Wu Luo, and 82270364 to Xiong Chen).

## Author contributions

Guang Liang and Xiaokun Li contributed to the literature search and study design. Guang Liang, Jinfu Qian, and Xiong Chen participated in the drafting of the article. Xiong Chen, Jinfu Qian, Wu Luo, Yujuan Shi, and Shiqi Liang carried out the experiments. Gaojun Wu, and Xiang Hu revised the manuscript. Hong Zhu, and Jianchang Qian contributed to data collection and analysis.

## Conflicts of interest

The authors declare no conflicts of interest.

## Appendix A. Supporting information

Supporting data to this article can be found online at <https://doi.org/10.1016/j.apsb.2024.01.013>.

## References

- Rubler S, Dlugash J, Yuceoglu YZ, Kumral T, Branwood AW, Grishman A. New type of cardiomyopathy associated with diabetic glomerulosclerosis. *Am J Cardiol* 1972;**30**:595–602.
- Ritchie RH, Abel ED. Basic mechanisms of diabetic heart disease. *Circ Res* 2020;**126**:1501–25.
- Marwick TH, Ritchie R, Shaw JE, Kaye D. Implications of underlying mechanisms for the recognition and management of diabetic cardiomyopathy. *J Am Coll Cardiol* 2018;**71**:339–51.
- Wei J, Zhao Y, Liang H, Du W, Wang L. Preliminary evidence for the presence of multiple forms of cell death in diabetes cardiomyopathy. *Acta Pharm Sin B* 2022;**12**:1–17.
- Wang X, Antony V, Wang Y, Wu G, Liang G. Pattern recognition receptor-mediated inflammation in diabetic vascular complications. *Med Res Rev* 2020;**40**:2466–84.
- Sanders-van Wijk S, Tromp J, Beussink-Nelson L, Hage C, Svedlund S, Saraste A, et al. Proteomic evaluation of the comorbidity-inflammation paradigm in heart failure with preserved ejection fraction: results from the PROMIS-HFpEF Study. *Circulation* 2020;**142**:2029–44.
- Roskoski Jr R. Properties of FDA-approved small molecule protein kinase inhibitors. *Pharmacol Res* 2019;**144**:19–50.

8. Grimminger F, Schermuly RT, Ghofrani HA. Targeting non-malignant disorders with tyrosine kinase inhibitors. *Nat Rev Drug Discov* 2010;**9**:956–70.
9. Zheng M, Zhang Q, Zhang C, Wu C, Yang K, Song Z, et al. A natural DYRK1A inhibitor as a potential stimulator for beta-cell proliferation in diabetes. *Clin Transl Med* 2021;**11**:e494.
10. Pucelik B, Barzowska A, Dabrowski JM, Czarna A. Diabetic kinase inhibitors—a new opportunity for  $\beta$ -cells restoration. *Int J Mol Sci* 2021;**22**:9083.
11. Fountas A, Diamantopoulos LN, Tsatsoulis A. Tyrosine kinase inhibitors and diabetes: a novel treatment paradigm?. *Trends Endocrinol Metabol* 2015;**26**:643–56.
12. Sheng L, Bayliss G, Zhuang S. Epidermal growth factor receptor: a potential therapeutic target for diabetic kidney disease. *Front Pharmacol* 2021;**11**:598910.
13. Galan M, Kassan M, Choi SK, Partyka M, Trebak M, Henrion D, et al. A novel role for epidermal growth factor receptor tyrosine kinase and its downstream endoplasmic reticulum stress in cardiac damage and microvascular dysfunction in type 1 diabetes mellitus. *Hypertension* 2012;**60**:71–80.
14. Liang D, Zhong P, Hu J, Lin F, Qian Y, Xu Z, et al. EGFR inhibition protects cardiac damage and remodeling through attenuating oxidative stress in STZ-induced diabetic mouse model. *J Mol Cell Cardiol* 2015;**82**:63–74.
15. Shraim BA, Moursi MO, Benter IF, Habib AM, Akhtar S. The role of epidermal growth factor receptor family of receptor tyrosine kinases in mediating diabetes-induced cardiovascular complications. *Front Pharmacol* 2021;**12**:701390.
16. Pacini L, Jenks AD, Lima NC, Huang PH. Targeting the fibroblast growth factor receptor (FGFR) family in lung cancer. *Cells* 2021;**10**:1154.
17. Yin F, Zhao R, Gorja DR, Fu X, Lu N, Huang H, et al. Novel dual inhibitor for targeting PIM1 and FGFR1 kinases inhibits colorectal cancer growth *in vitro* and patient-derived xenografts *in vivo*. *Acta Pharm Sin B* 2022;**12**:4122–37.
18. Meric-Bernstam F, Bahleda R, Hierro C, Sanson M, Bridgewater J, Arkenau HT, et al. Futibatinib, an irreversible FGFR1–4 inhibitor, in patients with advanced solid tumors harboring FGF/FGFR aberrations: a phase I dose-expansion study. *Cancer Discov* 2021;**12**:402–15.
19. Wu L, Zhang C, He C, Qian D, Lu L, Sun Y, et al. Discovery of pemigatinib: a potent and selective fibroblast growth factor receptor (FGFR) inhibitor. *J Med Chem* 2021;**64**:10666–79.
20. Wang S, Cao S, Arhatte M, Li D, Shi Y, Kurz S, et al. Adipocyte Piezo1 mediates obesogenic adipogenesis through the FGF1/FGFR1 signaling pathway in mice. *Nat Commun* 2020;**11**:2303.
21. Li J, Liu H, Srivastava SP, Hu Q, Gao R, Li S, et al. Endothelial FGFR1 (fibroblast growth factor receptor 1) deficiency contributes differential fibrogenic effects in kidney and heart of diabetic mice. *Hypertension* 2020;**76**:1935–44.
22. Raj T, Kanellakis P, Pomilio G, Jennings G, Bobik A, Agrotis A. Inhibition of fibroblast growth factor receptor signaling attenuates atherosclerosis in apolipoprotein E-deficient mice. *Arterioscler Thromb Vasc Biol* 2006;**26**:1845–51.
23. Wang Y, Qian Y, Fang Q, Zhong P, Li W, Wang L, et al. Saturated palmitic acid induces myocardial inflammatory injuries through direct binding to TLR4 accessory protein MD2. *Nat Commun* 2017;**8**:13997.
24. Ackers-Johnson M, Li PY, Holmes AP, O'Brien SM, Pavlovic D, Foo RS. A simplified, Langendorff-free method for concomitant isolation of viable cardiac myocytes and nonmyocytes from the adult mouse heart. *Circ Res* 2016;**119**:909–20.
25. Wang Y, Luo W, Han J, Khan ZA, Fang Q, Jin Y, et al. MD2 activation by direct AGE interaction drives inflammatory diabetic cardiomyopathy. *Nat Commun* 2020;**11**:2148.
26. Wu S, Lu Q, Ding Y, Wu Y, Qiu Y, Wang P, et al. Hyperglycemia-driven inhibition of AMP-activated protein kinase  $\alpha$ 2 induces diabetic cardiomyopathy by promoting mitochondria-associated endoplasmic reticulum membranes *in vivo*. *Circulation* 2019;**139**:1913–36.
27. Lu S, Liao Z, Lu X, Katschinski DM, Mercola M, Chen J, et al. Hyperglycemia acutely increases cytosolic reactive oxygen species via O-linked GlcNAcylation and CaMKII activation in mouse ventricular myocytes. *Circ Res* 2020;**126**:e80–96.
28. Beyrakhova K, Li L, Xu C, Gagarinova A, Cygler M. *Legionella pneumophila* effector Lem4 is a membrane-associated protein tyrosine phosphatase. *J Biol Chem* 2018;**293**:13044–58.
29. Mohammadi M, Dikic I, Sorokin A, Burgess WH, Jaye M, Schlessinger J. Identification of six novel autophosphorylation sites on fibroblast growth factor receptor 1 and elucidation of their importance in receptor activation and signal transduction. *Mol Cell Biol* 1996;**16**:977–89.
30. De S, Zhou H, DeSantis D, Croniger CM, Li X, Stark GR. Erlotinib protects against LPS-induced endotoxicity because TLR4 needs EGFR to signal. *Proc Natl Acad Sci U S A* 2015;**112**:9680–5.
31. Chattopadhyay S, Veleparambil M, Poddar D, Abdulkhalek S, Bandyopadhyay SK, Fensterl V, et al. EGFR kinase activity is required for TLR4 signaling and the septic shock response. *EMBO Rep* 2015;**16**:1535–47.
32. Jia G, Hill MA, Sowers JR. Diabetic cardiomyopathy: an update of mechanisms contributing to this clinical entity. *Circ Res* 2018;**122**:624–38.
33. Tan Y, Zhang Z, Zheng C, Wintergerst KA, Keller BB, Cai L. Mechanisms of diabetic cardiomyopathy and potential therapeutic strategies: preclinical and clinical evidence. *Nat Rev Cardiol* 2020;**17**:585–607.
34. Gavine PR, Mooney L, Kilgour E, Thomas AP, Al-Kadhimi K, Beck S, et al. AZD4547: an orally bioavailable, potent, and selective inhibitor of the fibroblast growth factor receptor tyrosine kinase family. *Cancer Res* 2012;**72**:2045–56.
35. Tsushima K, Bugger H, Wende AR, Soto J, Jenson GA, Tor AR, et al. Mitochondrial reactive oxygen species in lipotoxic hearts induce post-translational modifications of AKAP121, DRP1, and OPA1 that promote mitochondrial fission. *Circ Res* 2018;**122**:58–73.
36. Weekes D, Kashima TG, Zandueta C, Perurena N, Thomas DP, Sinters A, et al. Regulation of osteosarcoma cell lung metastasis by the c-Fos/AP-1 target FGFR1. *Oncogene* 2016;**35**:2852–61.
37. Saichaemchan S, Ariyawutyakorn W, Varella-Garcia M. Fibroblast growth factor receptors: from the oncogenic pathway to targeted therapy. *Curr Mol Med* 2016;**16**:40–62.
38. Gordon JW, Shaw JA, Kirshenbaum LA. Multiple facets of NF- $\kappa$ B in the heart: to be or not to NF- $\kappa$ B. *Circ Res* 2011;**108**:1122–32.
39. Fon Tacer K, Bookout AL, Ding X, Kurosu H, John GB, Wang L, et al. Research resource: comprehensive expression atlas of the fibroblast growth factor system in adult mouse. *Mol Endocrinol* 2010;**24**:2050–64.
40. Hughes SE. Differential expression of the fibroblast growth factor receptor (FGFR) multigene family in normal human adult tissues. *J Histochem Cytochem* 1997;**45**:1005–19.
41. Liang G, Song L, Chen Z, Qian Y, Xie J, Zhao L, et al. Fibroblast growth factor 1 ameliorates diabetic nephropathy by an anti-inflammatory mechanism. *Kidney Int* 2018;**93**:95–109.
42. Huang Z, Tan Y, Gu J, Liu Y, Song L, Niu J, et al. Uncoupling the mitogenic and metabolic functions of FGF1 by tuning FGF1–FGF receptor dimer stability. *Cell Rep* 2017;**20**:1717–28.
43. Wang D, Jin M, Zhao X, Zhao T, Lin W, He Z, et al. FGF1<sup>4HBS</sup> ameliorates chronic kidney disease via PI3K/AKT mediated suppression of oxidative stress and inflammation. *Cell Death Dis* 2019;**10**:464.
44. Wang D, Yin Y, Wang S, Zhao T, Gong F, Zhao Y, et al. FGF1<sup>4HBS</sup> prevents diabetic cardiomyopathy by maintaining mitochondrial homeostasis and reducing oxidative stress via AMPK/Nur77 suppression. *Signal Transduct Targeted Ther* 2021;**6**:133.

45. Novoyatleva T, Sajjad A, Pogoryelov D, Patra C, Schermuly RT, Engel FB. FGF1-mediated cardiomyocyte cell cycle reentry depends on the interaction of FGFR-1 and Fn14. *FASEB J* 2014;**28**:2492–503.
46. Cilvik SN, Wang JI, Lavine KJ, Uchida K, Castro A, Gierasch CM, et al. Fibroblast growth factor receptor 1 signaling in adult cardiomyocytes increases contractility and results in a hypertrophic cardiomyopathy. *PLoS One* 2013;**8**:e82979.
47. Wang C, Ke Y, Liu S, Pan S, Liu Z, Zhang H, et al. Ectopic fibroblast growth factor receptor 1 promotes inflammation by promoting nuclear factor- $\kappa$ B signaling in prostate cancer cells. *J Biol Chem* 2018;**293**:14839–49.
48. Akhtar S, Yousif MH, Chandrasekhar B, Benter IF. Activation of EGFR/ERBB2 via pathways involving ERK1/2, P38 MAPK, AKT and FOXO enhances recovery of diabetic hearts from ischemia–reperfusion injury. *PLoS One* 2012;**7**:e39066.
49. Luo W, Huang L, Wang J, Zhuang F, Xu Z, Yin H, et al. Inhibition of EGFR–STAT3 attenuates cardiomyopathy in streptozotocin-induced type 1 diabetes. *J Endocrinol* 2019;**242**:199–210.
50. Basu S, Pathak SK, Chatterjee G, Pathak S, Basu J, Kundu M. *Helicobacter pylori* protein HP0175 transactivates epidermal growth factor receptor through TLR4 in gastric epithelial cells. *J Biol Chem* 2008;**283**:32369–76.
51. Prabhu SD, Frangogiannis NG. The biological basis for cardiac repair after myocardial infarction: from inflammation to fibrosis. *Circ Res* 2016;**119**:91–112.
52. Mann DL. Innate immunity and the failing heart: the cytokine hypothesis revisited. *Circ Res* 2015;**116**:1254–68.
53. Kenny HC, Abel ED. Heart failure in type 2 diabetes mellitus. *Circ Res* 2019;**124**:121–41.
54. Lopez B, Ravassa S, Moreno MU, Jose GS, Beaumont J, Gonzalez A, et al. Diffuse myocardial fibrosis: mechanisms, diagnosis and therapeutic approaches. *Nat Rev Cardiol* 2021;**18**:479–98.
55. Frati G, Schirone L, Chimenti I, Yee D, Biondi-Zoccai G, Volpe M, et al. An overview of the inflammatory signalling mechanisms in the myocardium underlying the development of diabetic cardiomyopathy. *Cardiovasc Res* 2017;**113**:378–88.
56. Oduro PK, Zheng X, Wei J, Yang Y, Wang Y, Zhang H, et al. The cGAS–STING signaling in cardiovascular and metabolic diseases: future novel target option for pharmacotherapy. *Acta Pharm Sin B* 2022;**12**:50–75.